TECHNICAL REPORT ARBRL-TR-02168

A NEW INTERNAL ENERGY CALCULATION FOR THE HELP CODE AND ITS IMPLICATIONS TO CONICAL SHAPED CHARGE SIMULATIONS

James A. Schmitt

June 1979

US ARMY ARMAMENT RESEARCH AND DEVELOPMENT COMMAND
BALLISTIC RESEARCH LABORATORY
ABERDEEN PROVING GROUND, MARYLAND

Destroy this report when it is no longer needed.
Do not return it to the originator.

Secondary distribution of this report by originating or sponsoring activity is prohibited.

Additional copies of this report may be obtained from the National Technical Information Service, U.S. Department of Commerce, Springfield, Virginia 22161.

The findings in this report are not to be construed as an official Department of the Army position, unless so designated by other authorized documents.

The use of trade names or manufacturers' names in this report does not constitute indorsement of any commercial product.

UNCLASSIFIED

SECURITY CLASSIFICATION OF THIS PAGE (When Data Entered)

REPORT DOCUMENTATION PAGE		READ INSTRUCTIONS BEFORE COMPLETING FORM
1. REPORT NUMBER TECHNICAL REPORT ARBRL-TR-02168	2. GOVT ACCESSION NO.	3. RECIPIENT'S CATALOG NUMBER
4. TITLE (and Subtitle) A New Internal Energy Calculation for the HELP Code and Its Implications to Conical Shaped Charge Simulations		5. TYPE OF REPORT & PERIOD COVERED 6. PERFORMING ORG. REPORT NUMBER
7. AUTHOR(s) James A. Schmitt		8. CONTRACT OR GRANT NUMBER(s)
9. PERFORMING ORGANIZATION NAME AND ADDRESS US Army Ballistic Research Laboratory ATTN: DRDAR-BLB Aberdeen Proving Ground, MD 21005		10. PROGRAM ELEMENT, PROJECT, TASK AREA & WORK UNIT NUMBERS 1L161102AH63
11. CONTROLLING OFFICE NAME AND ADDRESS US Army Armament Research & Development Command Ballistic Research Laboratory (ATTN: DRDAR-BL) Aberdeen Proving Ground, MD 21005		12. REPORT DATE JUNE 1979 13. NUMBER OF PAGES 94
14. MONITORING AGENCY NAME & ADDRESS(if different from Controlling Office)		15. SECURITY CLASS. (of this report) Unclassified 15a. DECLASSIFICATION/DOWNGRADING SCHEDULE

16. DISTRIBUTION STATEMENT (of this Report)

Approved for public release; distribution unlimited.

17. DISTRIBUTION STATEMENT (of the abstract entered in Block 20, if different from Report)

18. SUPPLEMENTARY NOTES

19. KEY WORDS (Continue on reverse side if necessary and identify by block number)

HELP	HULL
HELP Code	Two-dimensional code
Hydrodynamic code	Eulerian
Particle-In-Cell	Numerical analysis
Finite difference solution technique	Truncation error

(OVER)

20. ABSTRACT (Continue on reverse side if necessary and identify by block number) (deh)

When the HELP code is applied to conical shaped charge warhead problems, the computed internal energy predicts a thermal state completely different than that indicated by experiments. The cause of this phenomenon is the numerical interchange of the kinetic energy to internal energy which is generated by terms of the order of the truncation error in the kinetic energy calculation. A correction is given and qualitative thermal agreement is achieved, for the first time,

(OVER)

DD FORM 1 JAN 73 1473 EDITION OF 1 NOV 65 IS OBSOLETE

UNCLASSIFIED

SECURITY CLASSIFICATION OF THIS PAGE (When Data Entered)

Block 19.

Mesh refinement	Shaped charge
Kinetic energy calculation	Conical shaped charge
Internal energy calculation	Wedge impact
Temperature calculation	Oblique impact

Block 20.

between a HELP code simulation and experimental evidence for a conical shaped charge. Furthermore, the ad hoc usage of a predetermined upper bound on the specific internal energy in the equation of state routine for shaped charge calculations is no longer required. The effects of the modifications on the pressures, velocities, specific total energies and densities are discussed.

The effect of the original kinetic energy calculation on the accuracy of the internal energy is problem dependent and criteria for such a determination are given in terms of the explicitly calculated truncation error terms for the specific internal energy. A mesh refinement study for a copper wedge impacting a perfectly reflexive wall is made using the original and modified versions of the code. The results not only show the tremendous deviations in the internal energies computed by the original version as the mesh is refined but also indicate that the internal energies computed by the modified version with a coarse mesh are better than those computed by the original version with a fine mesh. The same internal energy phenomenon which occurred in HELP can occur in other codes with a Particle-In-Cell based algorithm and the given correction is applicable.

TABLE OF CONTENTS

	Page
LIST OF FIGURES	5
LIST OF TABLES	7
I. INTRODUCTION	9
II. THE HELP CODE	10
III. THE KINETIC ENERGY AND INTERNAL ENERGY CALCULATIONS	18
IV. THE MODIFIED HELP CODE	29
V. MESH REFINEMENT STUDY FOR A WEDGE IMPACT CALCULATION	31
VI. COMPARISON OF THE MODIFIED AND ORIGINAL FORMULATIONS USING A 43MM CONICAL SHAPED CHARGE SIMULATION	36
VII. TEMPERATURE CALCULATIONS FOR THE 43MM CONICAL SHAPED CHARGE	52
VIII. SUMMARY	58
ACKNOWLEDGEMENT	60
REFERENCES	61
APPENDIX A - LISTING OF MODIFICATIONS TO THE KINETIC ENERGY CALCULATION IN HELP	65
APPENDIX B - LISTING OF REZONING ROUTINE AND MODIFICATIONS	77
APPENDIX C - LISTING OF TEMPERATURE AND SPECIAL PRINT ROUTINES	83
LIST OF SYMBOLS	87
DISTRIBUTION LIST	89

LIST OF FIGURES

Figure		Page
1	Computational Cell for Cartesian Formulation of HELP . .	13
2	Typical Time History Profile of the Internal Energy per Volume in a Conical Shaped Charge Calculation . . .	25
3	Typical Spatial Profiles of the Axial Velocity and Internal Energy per Volume in a Conical Shaped Charge Calculation	27
4	Spatial Profiles of the Relative Axial Velocity at 10μs Along the Wall for a Copper Wedge Impact Calculation	33
5	Spatial Profiles of the Compression at 10μs Along the Wall for a Copper Wedge Impact Calculation	34
6	Spatial Profiles of the Specific Internal Energy at 10μs Along the Wall for a Copper Wedge Impact Calculation	35
7a	Initial Conical Shaped Charge Configuration	37
7b	Copper Configuration at 16μs for Conical Shaped Charge .	37
8	Comparison of the Specific Kinetic Energies Along the Axis of Symmetry at 16μs	39
9	Comparison of the Specific Internal Energies Along the Axis of Symmetry at 16μs	40
10	Cell-Centered Values of the Jet's Specific Internal Energy (MJ/kg) Computed by the Modified Formulation . .	42
11	Modified Version's Specific Internal Energy Profiles from the Stagnation Region to the Jet Tip at Various Time	43
12	Comparison of the Pressures Along the Axis of Symmetry at 16μs	45
13	Comparison of the Axial Velocities Along the Axis of Symmetry at 16μs	46
14	Comparison of the Jet Tip Velocity-Time Histories . . .	47

Figure		Page
15	Comparison of the Radial Velocities Along the Axis of Symmetry at 16μs	48
16	Comparison of the Specific Total Energies Along the Axis of Symmetry at 16μs	49
17	Comparison of the Compressions Along the Axis of Symmetry at 16μs	50
18	Variation of Jet's Temperature with Axial Distance at Various Distances from the Axis of Symmetry at 16μs . .	56
19	Variation of Jet's Temperature with Axial Distance at Various Distances from the Axis of Symmetry at 18.5μs .	57

LIST OF TABLES

Table		Page
1	Density Variation Within the Jet at 16μs	54

I. INTRODUCTION

Time dependent two-dimensional Eulerian computer codes like HELP[1] and HULL[2] are utilized to describe the unsteady interactions of continuous media (fluid and/or solids). Many of these continuum codes have a common ancestorial algorithm, the Particle-In-Cell method[3,4,5]. During the evolutionary process, the new codes have deviated substantially from the original PIC method; for example, the discrete particles were replaced by a continuum, certain Lagrangian-type features were abandoned, and for calculations in solid mechanics, material strength and effects of the deviatoric stress tensor were included. These codes can produce very successful simulations but often the results are not totally satisfactory. Such is the case with the HELP code which is used by several research laboratories and corporations for diverse applications in compressible flow and elastic-plastic flows. In certain ballistics applications at the US Army Ballistics Research Laboratory, the code predicts velocities satisfactorily but an internal energy which implies a different thermal state than that indicated by experimental evidence. The purpose of this paper is to show that the original approximations in HELP lead to specific error terms that significantly and consistently influence the internal energy calculation and to propose a correction within the context of the current algorithm.

The internal energy algorithm in HELP is based on the finite difference approximation of the total energy equation and the kinetic energy calculated from updated mass and momentum values. This internal energy approximation is shown to include terms of the order of the truncation error which arise in the kinetic energy calculation from the finite difference approximations of the mass and momentum equations. These terms,

1. Hageman, L. J., et al., "HELP, A Multi-Material Eulerian Program for Compressible Fluid and Elastic-Plastic Flows in Two Space Dimensions and Time," Systems, Science and Software Report No. SSS-R-75-2654, July 1975.

2. Fry, M. A., et al., "The HULL Hydrodynamics Computer Code," Air Force Weapons Laboratory Report No. AFWL-TR-76-193, September 1976.

3. Evans, M. W. and Harlow, F. H., "The Particle-In-Cell Method for Hydrodynamic Calculations," Los Alamos Scientific Laboratory Report No. 2139, November 1957.

4. Harlow, F. H., "The Particle-In-Cell Computing Method for Fluid Dynamics," in Methods in Computational Physics, (B. Alder, S. Fernback and M. Rothenberg, eds.), Academic Press, New York, 1964.

5. Harlow, F. H., "The Particle-In-Cell Method for Numerical Solution of Problems in Fluid Dynamics," in Proceedings of Symposia in Applied Mathematics, Vol. XV, (N. Metropolis, J. Todd, A. Tank, C. Tompkins, eds.) American Mathematical Society, Providence, Rhode Island, 1963.

in certain cases, cause a less accurate calculation of the internal energy (they increase the truncation error) and produce an interchange of energy at each phase which is not modeled in the governing equations. Evans and Harlow[3] identified an energy transfer mechanism in the convection phase of the original PIC method which can be seen in HELP. This mechanism is due only to spatial discretization and was illustrated in one dimension. The following analysis involves all the phases in the HELP algorithm, is two-dimensional, includes the effect of time discretization, and applies to a different code with a different energy formulation (the PIC algorithm transports total energy but directly calculates the internal energy in its other phases). Although this paper deals exclusively with the HELP algorithm, the concepts and results discussed are applicable to other codes. In particular, the same internal energy phenomenon is seen in calculations performed with the HULL code.

In Section II, the governing equations which are modeled by the HELP algorithm are listed, the corresponding approximations are derived and other salient features of the algorithm are discussed. A truncation error analysis of the kinetic energy and the internal energy calculations in Section III reveals the specific error terms arising from the HELP's finite difference approximations of the governing equations. In Section IV, the modifications to the original HELP code are given and their implementation discussed. Section V contains a mesh refinement study for both the original and modified version of the code. A copper wedge impacting a perfectly reflective wall was used for this study. Section VI contains a detailed comparison of the two versions for 43mm unconfined conical shaped charge. Temperature profiles within the shaped charge jet are given and discussed in Section VII. The summary of the report is Section VIII.

II. THE HELP CODE

The unsteady motion and interaction of continuous media can be described by a continuity equation, equations of motion, a total energy equation and an equation of state. For simplicity, we shall consider the Cartesian formulation. The appropriate two-dimensional equations in conservative form are:

$$\frac{\partial \rho}{\partial t} = - \frac{\partial}{\partial x} (\rho u) - \frac{\partial}{\partial y} (\rho v), \tag{1}$$

$$\frac{\partial (\rho u)}{\partial t} = - \frac{\partial}{\partial x} (\rho u u) - \frac{\partial}{\partial y} (\rho v u) - \frac{\partial P}{\partial x} + \frac{\partial}{\partial x} (S_{xx}) + \frac{\partial}{\partial y} (S_{xy}), \tag{2}$$

$$\frac{\partial (\rho v)}{\partial t} = - \frac{\partial}{\partial x} (\rho u v) - \frac{\partial}{\partial y} (\rho v v) - \frac{\partial P}{\partial y} + \frac{\partial}{\partial x} (S_{xy}) + \frac{\partial}{\partial y} (S_{yy}), \tag{3}$$

$$\frac{\partial(\rho E)}{\partial t} = -\frac{\partial}{\partial x}(\rho u E) - \frac{\partial}{\partial y}(\rho v E) - \frac{\partial(uP)}{\partial x} - \frac{\partial(vP)}{\partial y}$$

$$+ \frac{\partial}{\partial x}(S_{xx}u + S_{xy}v) + \frac{\partial}{\partial y}(S_{yy}v + S_{xy}u), \tag{4}$$

where t, x, y, ρ, u, v, P, S_{xx}, S_{yy}, S_{xy}, and E denote the time, two spatial coordinates, density, x and y components of velocity, pressure, the two normal and one shear stress components of the stress deviator tensor, and specific total energy, respectively. The cgs system of units is used within the HELP code. However, in this report, the results are stated in the SI system of units. The elements of the stress deviator tensor are functions of the velocity gradient. The pressure is computed via an equation of state of the functional form $P = P(\rho, I)$, where I is the specific internal energy. The specific internal energy is obtained as the difference of the specific total energy and the specific kinetic energy:

$$I = E - 0.5\,(u^2 + v^2). \tag{5}$$

If the conservation eqs. (1) - (4) are integrated over an arbitrary control area, the time rate of change of a quantity within the control area can be related to the integrals of other quantities over the boundary enclosing that area. Performing the integration and using Green's Theorem, we obtain

$$\frac{\partial}{\partial t}\int_A \rho dA = \int_B (\rho v dx - \rho u dy), \tag{6}$$

$$\frac{\partial}{\partial t}\int_A \rho u dA = \int_B u(\rho v dx - \rho u dy) - \int_B P dy + \int_B (S_{xx}dy - S_{xy}dx), \tag{7}$$

$$\frac{\partial}{\partial t}\int_A \rho v dA = \int_B v(\rho v dx - \rho u dy) + \int_B P dx + \int_B (S_{xy}dy - S_{yy}dx), \tag{8}$$

$$\frac{\partial}{\partial t}\int_A \rho E dA = \int_B E(\rho v dx - \rho u dy) + \int_B (P v dx - P u dy)$$

$$+ \int_B \left[(S_{xx}u + S_{xy}v)dy - (S_{yy}v + S_{xy}u)\,dx\right], \tag{9}$$

where B is the boundary of area A in the positive sense. Eq. (7), for example, equates the time rate of change of the x-component of the momentum within the area A to the product of the specific momentum in the x direction and the net mass flow into the area plus the sum of certain surface forces (the pressure and the x-components of the deviator stress tensor) exerted over the boundary enclosing the area Such interpretations are used to determine the HELP approximations to the governing equations.

The HELP code is an Eulerian code capable of describing unsteady multi-material interactions and of treating material strength as an elastic-plastic phenomenon. A consequence of the multi-material capability is mixed cells (cells containing more than one material). The complex treatment of these cells is important and indispensable to the correct running of the code. However, an accurate and complete analysis of these numerical techniques is unwieldy. An analysis of the pure cell (a cell containing only one material) algorithm reveals the cause of the internal energy problem. Hence, the following discussion will address only the pure cell algorithm. Furthermore, we consider only interior cells. We assume that the grid spacing Δx in the x-direction is constant as well as Δy in the y-direction. The control area A is taken to be the i^{th}, j^{th} computational cell. See Fig. 1. The left, right, top and bottom boundaries of this cell are denoted by the letters ℓ, r, a and b, respectively. A time step Δt in this explicit algorithm is determined by a Courant condition. The area integrals in eqs. (6) - (9) are approximated by $m = \rho\Delta x\Delta y$, mu, mv and mE, respectively, where m denotes the mass per unit length. All the values are at the center of the computational cell. The time derivatives are approximated by a forward difference. The values of the cell centered mass, momentum and specific total energy at the new time level are found from the values at the previous time level. This is accomplished in three stages by determining the time rate of change of the mass, momentum and total energy due to i) the effects of the deviatoric stresses, ii) the effects of the pressure, and iii) the effects of the convection terms. These phases are appropriately named SPHASE, HPHASE and TPHASE, respectively. During each time step, each value of the mass, momentum and total energy is updated sequentially by each phase in the order listed and each phase uses the previously updated values as its initial values. Each phase is solved independently of the others and are interconnected only through the initial values. The boundary integrals in eqs. (6) - (9) are approximated using the current values of the integrands at the boundaries of the computational cell. The pressure is calculated before SPHASE and the stress deviator tensor is updated at the beginning of SPHASE. The internal energy is updated by eq. (5) at the end of each phase.

Specifically, we list the HELP approximations to the conservation of mass, momentum and total energy equations. The HELP approximations

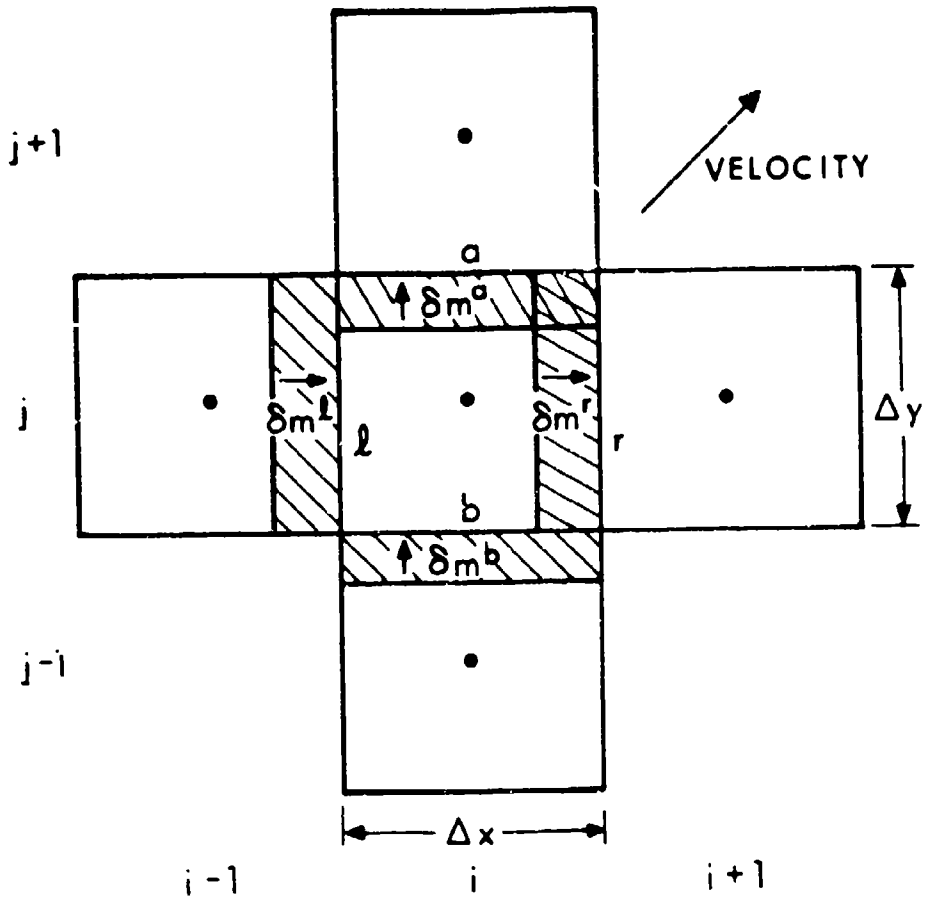

Figure 1. Computational Cell for Cartesian Formulation of HELP

to the eqs. (6) - (9) in the SPHASE portion of the calculation for the i^{th}, j^{th} cell at the n^{th} time step are:

$$\tilde{m} = m, \tag{10}$$

$$\tilde{mu} = mu + (S_{xx}{}^{r} - S_{xx}{}^{\ell})\Delta y\Delta t + (S_{xy}{}^{a} - S_{xy}{}^{b})\Delta x\Delta t, \tag{11}$$

$$\tilde{mv} = mv + (S_{xy}{}^{r} - S_{xy}{}^{\ell})\Delta y\Delta t + (S_{yy}{}^{a} - S_{yy}{}^{b})\Delta x\Delta t, \tag{12}$$

$$\begin{aligned}\tilde{mE} = mE &+ \left[(u^{r}S_{xx}{}^{r} - u^{\ell}S_{xx}{}^{\ell}) + (v^{r}S_{xy}{}^{r} - v^{\ell}S_{xy}{}^{\ell})\right]\Delta y\Delta t \\ &+ \left[(u^{a}S_{xy}{}^{a} - u^{b}S_{xy}{}^{b}) + (v^{a}S_{yy}{}^{a} - v^{b}S_{yy}{}^{b})\right]\Delta x\Delta t,\end{aligned} \tag{13}$$

where the tilde denotes the SPHASE updated value and the letter superscripts r, ℓ, a, b refer to the evaluation of the term at the corresponding boundary. A variable without subscripts or superscripts denotes that quantity evaluated at the center of the i^{th}, j^{th} cell at the n^{th} time level. The boundary value of a variable is the average of its cell centered values adjacent to that boundary, for example, $S^{r}_{xx} = 0.5$

$\left[(S_{xx})^{n}_{i+1,j} + (S_{xx})^{n}_{i,j}\right]$, where $(S_{xx})^{n}_{i,j} = S_{xx}\left[(i-\frac{1}{2})\Delta x, (j-\frac{1}{2})\Delta y, n\Delta t\right]$.

See Fig. 1. The approximations (10) - (13) can be derived from a physical interpretation of the SPHASE portions of eqs. (6) - (9). For example, consider the approximation (13). The effects of the stress deviator tensor on the time rate of change of the total energy $[\tilde{mE}-mE]/\Delta t$ during the entire time step Δt is governed by the work rates per unit surface area, uS_{xx} and vS_{xy} acting on the right and left boundaries and vS_{yy} and uS_{xy} on the top and the bottom boundaries, times the length of these boundaries.

The errors that are introduced by the numerical approximation (13) can be obtained by expanding the corresponding finite difference equation in a Taylor series. We use the mass-density relation $m = \rho\Delta x\Delta y$ and rewrite eq. (13) as

$$\frac{\widetilde{\rho E} - \rho E}{\Delta t} - \frac{u^r S_{xx}{}^r - u^\ell S_{xx}{}^\ell}{\Delta x} - \frac{v^r S_{xy}{}^r - v^\ell S_{xy}{}^\ell}{\Delta x} \tag{14}$$

$$- \frac{u^e S_{xy}{}^a - u^b S_{xy}{}^b}{\Delta y} - \frac{v^a S_{yy}{}^a - v^b S_{yy}{}^b}{\Delta y} = 0.$$

A Taylor series expansion of each dependent variable in eq. (14) at the center of the i^{th}, j^{th} cell at the n^{th} time level leads to

$$\frac{\partial(\rho E)}{\partial t} - \frac{\partial}{\partial x}\left[uS_{xx} + vS_{xy}\right] - \frac{\partial}{\partial y}\left[uS_{xy} + vS_{yy}\right] = -\Delta t\, \frac{1}{2}\left\{\frac{\partial^2(\rho E)}{\partial t^2}\right\}$$

$$- \Delta x^2\left\{\frac{1}{6}\frac{\partial^3}{\partial x^3}(uS_{xx} + vS_{xy}) - \frac{1}{4}\frac{\partial}{\partial x}\left(\frac{\partial u}{\partial x}\frac{\partial S_{xx}}{\partial x} + \frac{\partial v}{\partial x}\frac{\partial S_{xy}}{\partial x}\right)\right\} \tag{15}$$

$$- \Delta y^2\left\{\frac{1}{6}\frac{\partial^3}{\partial y^3}(uS_{xy} + vS_{yy}) - \frac{1}{4}\frac{\partial}{\partial y}\left(\frac{\partial u}{\partial y}\frac{\partial S_{xy}}{\partial y} + \frac{\partial v}{\partial y}\frac{\partial S_{yy}}{\partial y}\right)\right\}$$

$$+ O(\Delta t^2) + O(\Delta x^3) + O(\Delta y^3).$$

The terms in eq. (4) which are relevant to SPHASE are given on the left-hand side of eq. (15) and the dominant error terms appear on the right-hand side. The order of error terms are $O(\Delta t)$, $O(\Delta x^2)$ and $O(\Delta y^2)$. Thus, the approximation (13) is first order in time and second order in space within the context of SPHASE (assuming the post SPHASE values are those at the end of the time step). A similar analysis and results hold for approximations (11) - (12) and eqs. (2) - (3), respectively.

The HPHASE approximations are

$$\bar{m} = m, \tag{16}$$

$$\overline{mu} = m\tilde{u} - (P^r - P^\ell)\Delta y\Delta t, \tag{17}$$

$$\overline{mv} = m\tilde{v} - (P^a - P^b)\Delta x\Delta t, \tag{18}$$

$$\overline{mE} = m\tilde{E} - (P^r\tilde{u}^r - P^\ell\tilde{u}^\ell)\Delta y\Delta t - (P^a\tilde{v}^a - P^b\tilde{v}^b)\Delta x\Delta t, \tag{19}$$

where the bar denotes the HPHASE updated value and $P = P(\rho, I)$. The truncation error analysis of approximation (19) can be made in exactly the same manner as for approximation (13). The result is:

$$\begin{aligned}\frac{\partial(\tilde{\rho E})}{\partial t} + \frac{\partial(P\tilde{u})}{\partial x} + \frac{\partial(P\tilde{v})}{\partial y} &= -\Delta t\left\{\frac{1}{2}\frac{\partial^2(\tilde{\rho E})}{\partial t^2}\right\} - \Delta x^2\left\{\frac{1}{6}\frac{\partial^3}{\partial x^3}(P\tilde{u}) - \frac{1}{4}\frac{\partial}{\partial x}\left(\frac{\partial\tilde{u}}{\partial x}\frac{\partial P}{\partial x}\right)\right\} \\ &\quad - \Delta y^2\left\{\frac{1}{6}\frac{\partial^3}{\partial y^3}(P\tilde{v}) - \frac{1}{4}\frac{\partial}{\partial y}\left(\frac{\partial\tilde{v}}{\partial y}\frac{\partial P}{\partial y}\right)\right\} \\ &\quad + O(\Delta t^2) + O(\Delta x^3) + O(\Delta y^3).\end{aligned} \tag{20}$$

Thus eq. (19) is a first order approximation in time and second order in space within the context of HPHASE. The other HPHASE approximations (17) and (18) are of the same order.

For simplicity in the discussion of the TPHASE approximations, we assume that the velocity has both positive x and y components. The TPHASE approximations which model the convection between cells are:

$$m^{n+1} = m + \delta m^\ell - \delta m^r + \delta m^b - \delta m^a, \tag{21}$$

$$(mu)^{n+1} = m\tilde{u} + \delta m^\ell\tilde{u}_{i-1,j} - \delta m^r\tilde{u} + \delta m^b\tilde{u}_{i,j-1} - \delta m^a\tilde{u}, \tag{22}$$

$$(mv)^{n+1} = m\tilde{v} + \delta m^\ell\tilde{v}_{i-1,j} - \delta m^r\tilde{v} + \delta m^b\tilde{v}_{i,j-1} - \delta m^a\tilde{v}, \tag{23}$$

$$(mE)^{n+1} = m\tilde{E} + \delta m^\ell\tilde{E}_{i-1,j} - \delta m^r\tilde{E} + \delta m^b\tilde{E}_{i,j-1} - \delta m^a\tilde{E} \tag{24}$$

where δm^{ℓ}, δm^{b}, δm^{r}, δm^{a} denote the convected mass per unit length from the left and bottom cells and to the right and top cells, respectively. See Fig. 1. In general, $\delta m^{d} = \rho^{d} L^{d} \bar{u}^{d} \Delta t$, where ρ^{d} denotes the density of the cell from which the mass is transported, $\bar{u}^{d}$ is the interpolated value of the velocity component normal to the cell boundary and L^{d} is the length of the cell boundary through which the mass is moved. For example, the factors in δm^{ℓ} are $\rho^{\ell} = \rho_{i-1,j}$, $\bar{u}^{\ell} = 0.5\ (\bar{u}+\bar{u}_{i-1,j})/\left[1+\Delta t(\bar{u} - \bar{u}_{i-1,j})/\Delta x\right]$ and $L^{\ell} = \Delta y$. We note that $\bar{u}^{d}$ represents the transport velocity of δm^{d} based on linear approximations over the time step Δt. The intuitive explanation of the TPHASE approximations for eq. (21) is that the mass at the end of TPHASE (the final value at (n+1) time level) is the mass originally in the cell plus the mass transported into the cell (δm^{ℓ}, δm^{b}) minus the mass transported from the cell (δm^{r}, δm^{a}). For the total energy approximation (24), a similar situation exists, except that now each convected mass is associated with the specific total energy of its "donor" cell. Within the context of TPHASE (assuming the post HPHASE values are the initial values at the n^{th} time time level), the approximations (21) - (24) can be shown to be first order in time and space to the TPHASE portions of eqs. (1) - (4), respectively. For example, to determine the order of approximation (24), we substitute the appropriate mass approximations and obtain

$$\frac{(\rho E)^{n+1} - (\rho \bar{E})}{\Delta t} + \frac{(\rho \bar{E})\bar{u}^{r} - (\rho_{i-1,j}\bar{E}_{i-1,j})\bar{u}^{\ell}}{\Delta x} + \frac{(\rho \bar{E})\bar{v}^{a} - (\rho_{i,j-1}\bar{E}_{i,j-1})\bar{v}^{b}}{\Delta y} = 0 \tag{25}$$

A Taylor series expansion of each dependent variable in eq. (25) at the center of the i^{th}, j^{th} cell at the n^{th} time level leads to

$$\frac{\partial(\overline{\rho E})}{\partial t} + \frac{\partial(\rho \overline{Eu})}{\partial x} + \frac{\partial(\rho \overline{Ev})}{\partial y} = -\frac{\Delta t}{2}\left[\frac{\partial^2(\rho \bar{E})}{\partial t^2} - 2\frac{\partial}{\partial x}\left(\rho \overline{Eu}\,\frac{\partial \bar{u}}{\partial x}\right) - 2\frac{\partial}{\partial y}\left(\rho \overline{Ev}\,\frac{\partial \bar{v}}{\partial y}\right)\right] + \frac{\Delta x}{2}\left[\frac{\partial}{\partial x}\left(\bar{u}\,\frac{\partial \rho \bar{E}}{\partial x}\right)\right] + \frac{\Delta y}{2}\left[\frac{\partial}{\partial y}\left(\bar{v}\,\frac{\partial \rho \bar{E}}{\partial y}\right)\right] + O(\Delta t^2) + O(\Delta x^2) + O(\Delta y^2). \tag{26}$$

The terms in eq. (4) which are relevant to TPHASE are given on the left-hand side of eq. (26) and the dominant error terms appear on the right-hand side. The spatial gradients in the coefficient of Δt in eq. (26) are the results of the transport velocities' $\bar{u}^r$, $\bar{u}^\ell$, $\bar{v}^a$ and $\bar{v}^b$ dependence on Δt. The order of the error terms are $O(\Delta t)$, $O(\Delta x)$ and $O(\Delta y)$. Thus, approximation (24) is first order in both time and space, which establishes the assertion.

We have shown that the SPHASE and HPHASE approximations of eqs. (1) - (4) are first order in time and second order in space and that the TPHASE approximations are first order in both time and space. Consequently, the order of the spatial approximation in TPHASE is less than that for either SPHASE or HPHASE and first order error terms will be dominant within the algorithm.

III. THE KINETIC ENERGY AND INTERNAL ENERGY CALCULATIONS

In order to determine the cause of the unphysical internal energy values produced by the 1975 HELP code in conical shaped charge calculations, we must investigate how the total energy approximations are combined with the kinetic energy approximations to produce the internal energy approximations. To this end we list the partial differential equations for the kinetic and internal energies. The partial differential equation governing kinetic energy can be derived from eqs. (1) - (3) by the following identity:

$$\frac{\partial}{\partial t}(\rho e) = u\frac{\partial \rho u}{\partial t} + v\frac{\partial \rho v}{\partial t} - \frac{1}{2}(u^2+v^2)\frac{\partial \rho}{\partial t}, \tag{27}$$

and can be written as

$$\begin{aligned}\frac{\partial}{\partial t}(\rho e) = &-\frac{\partial}{\partial x}(\rho u e) - \frac{\partial}{\partial y}(\rho v e) - u\frac{\partial P}{\partial x} - v\frac{\partial P}{\partial y} \\ &+ u\left(\frac{\partial S_{xx}}{\partial x} + \frac{\partial S_{xy}}{\partial y}\right) + v\left(\frac{\partial S_{xy}}{\partial x} + \frac{\partial S_{yy}}{\partial y}\right),\end{aligned} \tag{28}$$

where $e = 0.5\,(u^2 + v^2)$. An interpretation of the above manipulation is that given the exact solutions of eqs. (1) - (3), the derived function e is identical to the exact solution of eq. (28). We shall show that the HELP approximations do not share this property. The partial differential equation governing internal energy can be obtained by subtracting eq. (28) from eq. (4) and by using identity (5):

$$\frac{\partial}{\partial t}(\rho I) = -\frac{\partial}{\partial x}(\rho Iu) - \frac{\partial}{\partial y}(\rho Iv) - P\frac{\partial u}{\partial x} - P\frac{\partial v}{\partial y}$$

$$+ S_{xx}\frac{\partial u}{\partial x} + S_{xy}\left(\frac{\partial v}{\partial x} + \frac{\partial u}{\partial y}\right) + S_{yy}\frac{\partial v}{\partial y}. \tag{29}$$

In the HELP code, the specific kinetic energy e at the end of each phase is computed via

$$e = 0.5\left\{\left[(mu)/m\right]^2 + \left[(mv)/m\right]^2\right\} \tag{30}$$

using the updated values of the mass and momentum from that phase. By using the approximations (10) - (12), (16) - (18) and (21) - (23), eq. (30) and the expressions for the mass in terms of the density, we can write the formulas used to determine the updated specific kinetic energy at the different phases in terms of the initial values at SPHASE, HPHASE and TPHASE. The resulting expressions are never explicitly used to calculate the kinetic energy but are numerically equivalent to eq. (30). The results are:

$$\frac{(\tilde{\rho e})-\rho e}{\delta t} = u\left[\frac{S_{xx}^{\ r}-S_{xx}^{\ \ell}}{\Delta x} + \frac{S_{xy}^{\ a}-S_{xy}^{\ b}}{\Delta y}\right] + v\left[\frac{S_{xy}^{\ r}-S_{xy}^{\ \ell}}{\Delta x} + \frac{S_{yy}^{\ a}-S_{yy}^{\ b}}{\Delta y}\right]$$

$$+ \left\{\frac{\Delta t}{2\rho}\left[\left(\frac{S_{xx}^{\ r}-S_{xx}^{\ \ell}}{\Delta x} + \frac{S_{xy}^{\ a}-S_{xy}^{\ b}}{\Delta y}\right)^2 + \left(\frac{S_{xy}^{\ r}-S_{xy}^{\ \ell}}{\Delta x} + \frac{S_{yy}^{\ a}-S_{yy}^{\ b}}{\Delta y}\right)^2\right]\right\} \tag{31}$$

$$\frac{(\rho\bar{e}) - (\tilde{\rho e})}{\Delta t} = -\tilde{u}\left[\frac{p^r - p^\ell}{\Delta x}\right] - \tilde{v}\left[\frac{p^a - p^b}{\Delta y}\right]$$

$$+ \left\{\frac{\Delta t}{2\rho}\left[\left(\frac{p^r - p^\ell}{\Delta x}\right)^2 + \left(\frac{p^a - p^b}{\Delta y}\right)^2\right]\right\}, \tag{32}$$

$$\frac{(\rho e)^{n+1} - (\overline{\rho e})}{\Delta t} = - \frac{\rho \bar{u}^r \bar{e} - \rho_{i-1,j} \bar{u}^{\ell} \bar{e}_{i-1,j}}{\Delta x} - \frac{\rho \bar{v}^a \bar{e} - \rho_{i,j-1} \bar{v}^b \bar{e}_{i,j-1}}{\Delta y}$$

$$- \left\{ \frac{\rho_{i-1,j} \rho}{2\rho^{n+1}} \bar{u}^{\ell} \left[\Delta x - \bar{u}^r \Delta t - \bar{v}^a \Delta t \frac{\Delta x}{\Delta y} \right] \left[\left(\frac{\bar{u} - \bar{u}_{i-1,j}}{\Delta x} \right)^2 + \left(\frac{\bar{v} - \bar{v}_{i-1,j}}{\Delta x} \right)^2 \right] \right.$$

$$+ \frac{\rho_{i,j-1} \rho^{\bar{b}}}{2\rho^{n+1}} \left[\Delta y - \bar{v}^a \Delta t - \bar{u}^r \Delta t \frac{\Delta x}{\Delta y} \right] \left[\left(\frac{\bar{u} - \bar{u}_{i,j-1}}{\Delta y} \right)^2 + \left(\frac{\bar{v} - \bar{v}_{i,j-1}}{\Delta y} \right)^2 \right] \quad (33)$$

$$+ \frac{\rho_{i-1,j} \rho_{i,j-1} \bar{v}^b \bar{u}^{\ell}}{2\rho^{n+1}} \Delta t \frac{\Delta x}{\Delta y} \left[\left(\frac{\Delta y}{\Delta x} \frac{\bar{u} - \bar{u}_{i,j-1}}{\Delta y} - \frac{\bar{u} - \bar{u}_{i-1,j}}{\Delta x} \right)^2 \right.$$

$$\left. \left. + \left(\frac{\Delta y}{\Delta x} \frac{\bar{v} - \bar{v}_{i,j-1}}{\Delta y} - \frac{\bar{v} - \bar{v}_{i-1,j}}{\Delta x} \right)^2 \right] \right\}.$$

A truncation error analysis of eqs. (31) - (33) reveals significant information about the kinetic energy approximations. Since we have shown that the dominant error terms within the HELP algorithm are of first order, we will not write the higher order terms. Proceeding in a similar fashion to the truncation error analyses of Section II, we obtain for eq. (31)

$$\frac{\partial(\rho e)}{\partial t} - u \left(\frac{\partial S_{xx}}{\partial x} + \frac{\partial S_{xy}}{\partial y} \right) - v \left(\frac{\partial S_{xy}}{\partial x} + \frac{\partial S_{yy}}{\partial y} \right)$$

$$= - \frac{\Delta t}{2} \left[\frac{\partial^2 (\rho e)}{\partial t^2} - \frac{1}{\rho} \left(\frac{\partial S_{xx}}{\partial x} + \frac{\partial S_{xy}}{\partial y} \right)^2 - \frac{1}{\rho} \left(\frac{\partial S_{xy}}{\partial x} + \frac{\partial S_{yy}}{\partial y} \right)^2 \right] \quad (34)$$

$$+ O(\Delta t^2) + O(\Delta x^2) + O(\Delta y^2).$$

The terms in eq. (28) which are relevant to SPHASE are given on the left-hand side of eq. (34) and the dominant error terms appear on the right-hand side. The order of the error terms are $O(\Delta t)$, $O(\Delta x^2)$ and $O(\Delta y^2)$. Thus, approximation (31) is first order in time and second order in space, and the order of this approximation is consistent with the other SPHASE approximations. The terms

$$+ \frac{\Delta t}{2\rho}\left[\left(\frac{\partial S_{xx}}{\partial x} + \frac{\partial S_{xy}}{\partial y}\right)^2 + \left(\frac{\partial S_{xy}}{\partial x} + \frac{\partial S_{yy}}{\partial y}\right)^2\right]$$

in eq. (34) are the lowest order terms of those enclosed by braces in eq. (31). Thus, the braced terms in eq. (31) which are included in the kinetic energy approximation in SPHASE are of the order of the truncation error.

An analogous truncation error analysis of eq. (32) and eq. (33) gives, for HPHASE

$$\frac{\partial(\tilde{\rho e})}{\partial t} + \tilde{u}\frac{\partial P}{\partial x} + \tilde{v}\frac{\partial P}{\partial y} =$$

$$- \frac{\Delta t}{2}\left\{\frac{\partial^2(\tilde{\rho e})}{\partial t^2} - \frac{1}{\rho}\left(\frac{\partial P}{\partial x}\right)^2 - \frac{1}{\rho}\left(\frac{\partial P}{\partial y}\right)^2\right\} \qquad (35)$$

$$+ O(\Delta t^2) + O(\Delta x^2) + O(\Delta y^2),$$

and for TPHASE

$$\frac{\partial(\overline{\rho e})}{\partial t} + \frac{\partial}{\partial x}(\rho\overline{eu}) + \frac{\partial}{\partial y}(\rho\overline{ev}) =$$

$$+ \frac{\Delta x}{2}\left\{\frac{\partial}{\partial x}\left[\bar{u}\frac{\partial(\rho\bar{e})}{\partial x}\right] - \rho\bar{u}\left[\left(\frac{\partial\bar{u}}{\partial x}\right)^2 + \left(\frac{\partial\bar{v}}{\partial x}\right)^2\right]\right\}$$

$$+ \frac{\Delta y}{2}\left\{\frac{\partial}{\partial y}\left[\bar{v}\frac{\partial(\rho\bar{e})}{\partial y}\right] - \rho\bar{v}\left[\left(\frac{\partial\bar{u}}{\partial y}\right)^2 + \left(\frac{\partial\bar{v}}{\partial y}\right)^2\right]\right\} \qquad (36)$$

$$- \frac{\Delta t}{2}\left\{\frac{\partial^2(\overline{\rho e})}{\partial t^2} - 2\frac{\partial}{\partial x}\left(\bar{u}\rho\bar{e}\frac{\partial\bar{u}}{\partial x}\right) - 2\frac{\partial}{\partial y}\left(\bar{u}\rho\bar{e}\frac{\partial\bar{v}}{\partial y}\right)\right.$$

$$- \rho\bar{u}\left(\bar{u} + \bar{v}\frac{\Delta x}{\Delta y}\right)\left[\left(\frac{\partial\bar{u}}{\partial x}\right)^2 + \left(\frac{\partial\bar{v}}{\partial x}\right)^2\right] - \rho\bar{v}\left(\bar{v} + \bar{u}\frac{\Delta x}{\Delta y}\right)\left[\left(\frac{\partial u}{\partial y}\right)^2 + \left(\frac{\partial v}{\partial y}\right)^2\right]$$

$$\left. + \rho\overline{vu}\frac{\Delta x}{\Delta y}\left[\left(\frac{\Delta y}{\Delta x}\frac{\partial\bar{u}}{\partial y} - \frac{\partial\bar{u}}{\partial x}\right)^2 + \left(\frac{\Delta y}{\Delta x}\frac{\partial\bar{v}}{\partial y} - \frac{\partial\bar{v}}{\partial x}\right)^2\right]\right\}.$$

As in SPHASE, the HPHASE kinetic energy approximation is first order in time and second order in space, and includes terms (those enclosed in braces in eq. (32)) which are of the order of the truncation error. Eq. (36) shows that the TPHASE kinetic energy approximation is first order in both time and space. The terms enclosed in braces in eq. (33) contribute only to the $O(\Delta x)$, $O(\Delta y)$, $O(\Delta t)$ and higher order terms in eq. (36) and, consequently, are of the order of the truncation error.

Thus, the order of the approximations (31) - (33) are in accord with the other approximations in the three phases but these approximations include terms which are of the order of the truncation error: terms of order Δt is SPHASE and HPHASE and order Δt, Δx and Δy in TPHASE. These terms are consequences of calculating the kinetic energy from eq.(30) and from the particular choices made in the finite difference approximations of the mass and momentum equations in each phase. Furthermore, these terms do not model any term of the kinetic energy equation. In fact, if one would write directly a finite difference approximation to eq. (28) in a consistent manner with the HELP approximations of eqs. (1) - (4), the result would be eqs. (31) - (33) without the braced terms. Thus, the kinetic energy finite difference solutions within HELP do not share the corresponding property possessed by the exact solution of the partial differential equations: that is, the function e, eq. (30), derived from the finite difference solutions of the mass and momentum equations does not satisfy the finite difference approximation of eq. (28). Although the two approximations are the same in the theoretical limit as the mesh approaches zero, in practice the inclusion of terms of the order of the truncation error alters the accuracy of the calculation and the computed value.

By casing the above concepts into the framework of averaged quantities and fluctuations from their averages, an insight can be achieved into the nature of the truncation error terms. Consider an averaging procedure such that the average of the sum is the sum of the averages, the average of the average is the average and the average of a fluctuation is zero. The exact velocity can be written as the sum of the averaged velocity (doubled barred quantity) plus its fluctuation (primed quantity). Componentwise, we have

$$u = \bar{\bar{u}} + u' \quad \text{and} \quad v = \bar{\bar{v}} + v' .$$

The associated specific kinetic energy is

$$0.5(u^2 + v^2) = 0.5(\bar{\bar{u}}^2 + \bar{\bar{v}}^2) + 0.5(u'^2 + u'^2) + (\bar{\bar{u}}\, u' + \bar{\bar{v}}\, u'). \qquad (37)$$

Using the properties of the averaging procedure, we can write the average of eq. (37) as

$$\overline{0.5(u^2 + u^2)} - 0.5(\bar{\bar{u}}^2 + \bar{\bar{v}}^2) = \overline{0.5(u'^2 + v'^2)}. \qquad (38)$$

The difference between the averaged exact specific kinetic energy and the specific kinetic energy of the averaged velocities is the averaged specific kinetic energy of the fluctuations which can be called the subgrid-scale specific kinetic energy. If we take the averaged values as the computed cell centered values at the end of a single time step, then the first term on the left hand side of eq. (30) can be associated with the specific kinetic energy computed via the finite difference approximation of eq. (28) to a given order of accuracy and the second term with the specific kinetic energy computed via the cell centered values of the mass and momentum. Consider, for example, the TPHASE approximation to the specific kinetic energy. Eq. (33) can be rewritten in terms of the averaged values as

$$0.5(\bar{u}^2 + \bar{v}^2) = \overline{0.5(u^2 + v^2)} - \frac{\Delta t}{\rho^{n+1}} \left\{\text{truncation error terms}\right\}. \quad (39)$$

Comparing eq. (38) with eq. (39), we obtain

$$\overline{0.5(u'^2 + v'^2)} = \frac{\Delta t}{\rho^{n+1}} \left\{\text{truncation error terms}\right\}. \quad (40)$$

From eqs. (40) and (39), we see that the original formulation of HELP excludes the subgrid-scale kinetic energy. Accordingly, the direct calculation of the kinetic energy from eq. (28) includes it.

The effect of these truncation error terms is not confined to the kinetic energy calculation but is directly translated to the internal energy calculation via eq. (5). The accuracy of the internal energy calculation is of prime importance, since the pressure, temperature and strength properties of the material directly depend on the internal energy and not on either the total or kinetic energies. The dominant errors of the internal energy approximations in SPHASE can be seen by subtracting eq. (34) from eq. (15), in HPHASE by subtracting eq. (35) from eq. (20) and in TPHASE by subtracting eq. (36) from eq. (26). The results are for SPHASE,

$$\frac{\partial(\rho I)}{\partial t} - S_{xx}\frac{\partial u}{\partial x} - S_{xy}\left(\frac{\partial u}{\partial y} + \frac{\partial v}{\partial x}\right) - S_{yy}\frac{\partial v}{\partial y}$$

$$= -\frac{\Delta t}{2}\left[\frac{\partial^2(\rho I)}{\partial t^2} + \frac{1}{\rho}\left(\frac{\partial S_{xx}}{\partial x} + \frac{\partial S_{xy}}{\partial y}\right)^2 + \frac{1}{\rho}\left(\frac{\partial S_{xy}}{\partial x} + \frac{\partial S_{yy}}{\partial y}\right)^2\right] \quad (41)$$

$$+ O(\Delta t^2) + O(\Delta x^2) + O(\Delta y^2),$$

for HPHASE

$$\frac{\partial(\rho\tilde{I})}{\partial t} + P\left(\frac{\partial\tilde{u}}{\partial x} + \frac{\partial\tilde{v}}{\partial y}\right) = -\frac{\Delta t}{2}\left[\frac{\partial^2(\rho\tilde{I})}{\partial t^2} + \frac{1}{\rho}\left(\frac{\partial P}{\partial x}\right)^2 + \frac{1}{\rho}\left(\frac{\partial P}{\partial y}\right)^2\right] + O(\Delta t^2) + O(\Delta x^2) + O(\Delta y^2), \tag{42}$$

for TPHASE

$$\begin{aligned}\frac{\partial(\rho\bar{I})}{\partial t} + \frac{\partial(\rho\overline{Iu})}{\partial x} + \frac{\partial(\rho\overline{Iv})}{\partial y} &= \frac{\Delta x}{2}\left\{\frac{\partial}{\partial x}\left[\bar{u}\,\frac{\partial(\rho\bar{I})}{\partial x}\right] + \rho\overline{u}\left[\left(\frac{\partial\tilde{u}}{\partial x}\right)^2 + \left(\frac{\partial\tilde{v}}{\partial x}\right)^2\right]\right\} \\ &+ \frac{\Delta y}{2}\left\{\frac{\partial}{\partial y}\left[\bar{v}\,\frac{\partial(\rho\bar{I})}{\partial y}\right] + \rho\overline{v}\left[\left(\frac{\partial\tilde{u}}{\partial y}\right)^2 + \left(\frac{\partial\tilde{v}}{\partial y}\right)^2\right]\right\} \\ &- \frac{\Delta t}{2}\left\{\frac{\partial^2(\overline{\rho I})}{\partial t^2} - 2\,\frac{\partial}{\partial x}\left(\rho\overline{Iu}\,\frac{\partial\tilde{u}}{\partial x}\right) - 2\,\frac{\partial}{\partial y}\left(\rho\overline{Iv}\,\frac{\partial\tilde{v}}{\partial y}\right)\right. \\ &- \left.\bar{\rho}\left[\left(\bar{u}\,\frac{\partial\tilde{u}}{\partial x} + \bar{v}\,\frac{\partial\tilde{u}}{\partial y}\right)^2 + \left(\bar{u}\,\frac{\partial\tilde{v}}{\partial x} + \bar{v}\,\frac{\partial\tilde{v}}{\partial y}\right)^2\right]\right\} \\ &+ O(\Delta t^2) + O(\Delta x^2) + O(\Delta y^2),\end{aligned} \tag{43}$$

where we have assumed $\Delta x = \Delta y$ in order to simplify the TPHASE $O(\Delta t)$ term. The accuracy of the internal energy calculation depends primarily on the magnitude of the first order terms. The larger these terms are, the less accurate is the calculation. The structures of the first order terms in SPHASE and HPHASE are similar: a second time derivative of (ρI) plus positive terms which are a consequence of the truncation error terms in the kinetic energy calculation. These positive terms could be excluded from the kinetic energy calculation, and hence the internal energy calculation, without changing the order of the truncation error of the HELP algorithm. When the second time derivative of (ρI) is nonnegative, the SPHASE and HPHASE internal energy values are computed with less accuracy than would occur if these truncation error terms were excluded. A typical time history of the quantity (ρI) for a conical shaped change simulation (see Section IV) is given in Fig. 2. The curvature of this graph is nonnegative except for a short interval corresponding to the stagnation region within a shaped charge. Thus, at least for significant portions of a shaped change simulation, the internal energy calculation in SPHASE and HPHASE is less accurate

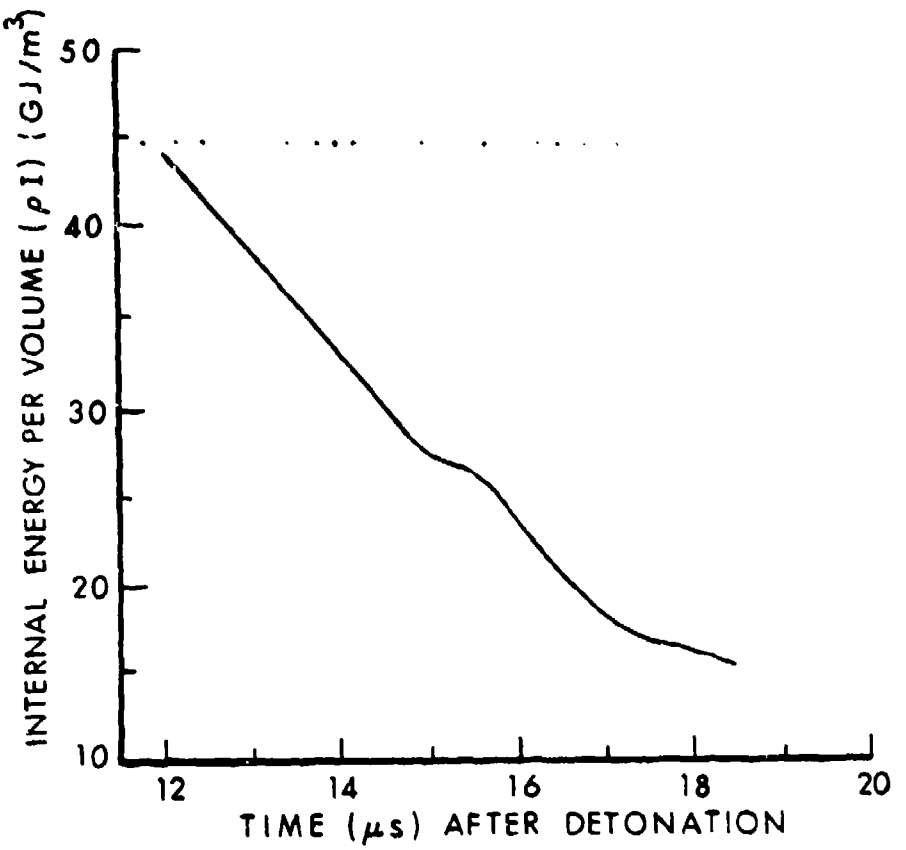

Figure 2. Typical Time History Profile of the Internal Energy per Volume in a Conical Shaped Charge Calculation

because of the inclusion of the truncation error terms from the kinetic energy calculation. Furthermore, even if the curvature of (ρI) with respect to time was negative, the accuracy of the internal energy may still be less if the order of magnitude of the sum of the squared items is greater than the curvature term.

In the TPHASE calculation, each of three first order terms in eq. (43) should be analyzed to ascertain the effects of the truncation error terms from the kinetic energy calculation (the squared terms in eq. (43)) on the internal energy calculation. In shaped charge simulations, the $O(\Delta y)$ term dominates the $O(\Delta x)$ and $O(\Delta t)$ terms, since the velocity and direction of the rate of change is primarily in the y direction and since a fairly coarse spatial computing mesh must be used ($O(\Delta y) \approx 10^{-2}$ versus $O(\Delta t) \approx 10^{-8}$). Hence, we consider only the $O(\Delta y)$ term, which we rewrite as:

$$\frac{\partial \bar{v}}{\partial y} \frac{\partial(\rho \bar{I})}{\partial y} + \bar{v} \frac{\partial^2(\rho \bar{I})}{\partial y^2} + \rho \bar{v} \left[\left(\frac{\partial \bar{u}}{\partial y} \right)^2 + \left(\frac{\partial \bar{v}}{\partial y} \right)^2 \right] . \tag{44}$$

Typical spatial profiles in shaped charge calculations of the quantities v and (ρI) along the axis of symmetry are given in Fig. 3. Since v is always positive and $\frac{\partial v}{\partial y}$, $\frac{\partial(\rho I)}{\partial y}$ and $\frac{\partial^2(\rho I)}{\partial y^2}$ are nonnegative throughout most of their variation, the sum of the first two terms is generally nonnegative. Consequently, since the third and fourth terms are always positive, the accuracy of the internal energy calculation is decreased. Thus, as was seen in the SPHASE and HPHASE approximations, the internal energy calculation for shaped charge calculations would generally be more accurate, if the truncation error terms from the kinetic energy calculation were excluded.

Another example of a flow in which the truncation error terms in the kinetic energy calculation would severely affect the internal energy calculation is in the expansion of perfect gas in a uniform pressure field. For a perfect gas, we have the relation $\rho I = P(\gamma - 1)^{-1}$ where the constant γ is the ratio of specific heats. Consequently, in a uniform pressure field, the quantities $\frac{\partial^2(\rho I)}{\partial t^2}$, $\frac{\partial(\rho I)}{\partial x}$, $\frac{\partial(\rho I)}{\partial y}$ would be zero in eqs. (41)-(43). If the truncation error terms from the kinetic energy calculation were excluded, the entire $O(\Delta t)$ term in SPHASE would be zero as well as the entire $O(\Delta x)$ and $O(\Delta y)$ terms in TPHASE. Thus the internal energy approximations in SPHASE would be $O(\Delta t^2)$ and TPHASE $O(\Delta x^2)$ and $O(\Delta y^2)$. Consequently, the approximations achieve a higher order of accuracy when the extraneous terms are excluded.

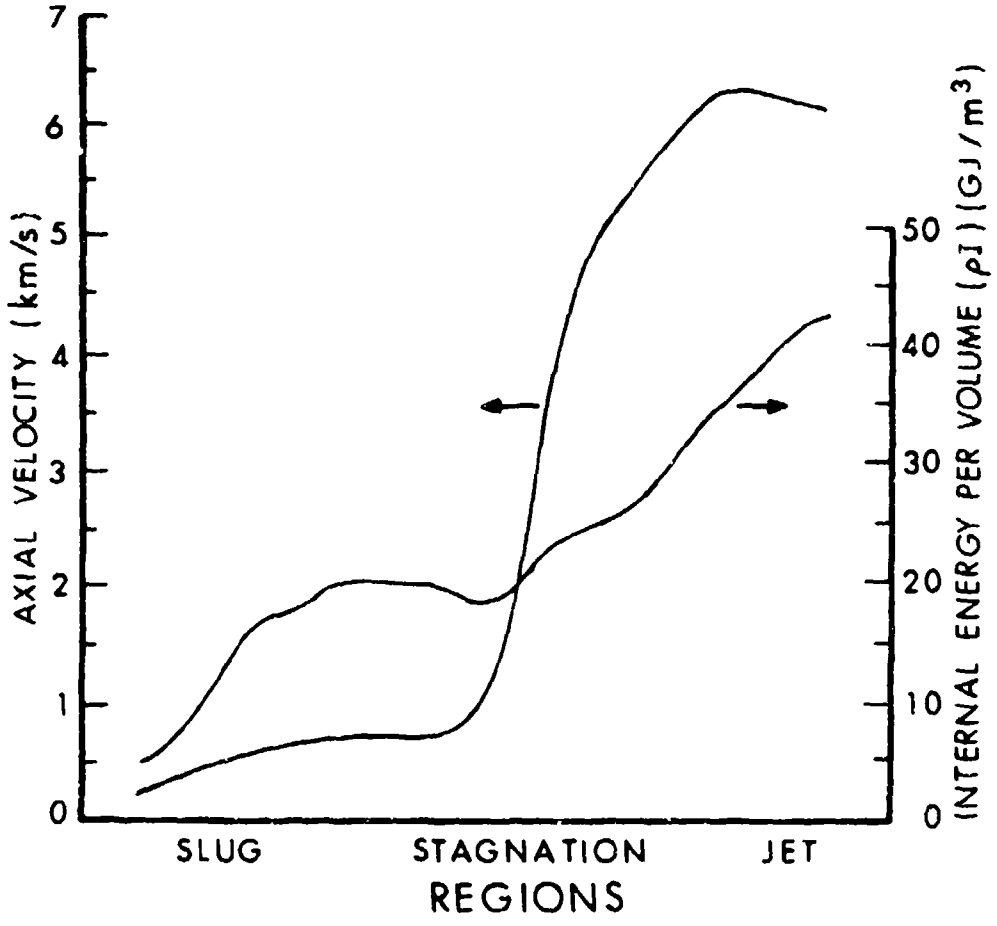

Figure 3. Typical Spatial Profiles of the Axial Velocity and Internal Energy per Volume in a Conical Shaped Charge Calculation

In other applications, the order of magnitude and/or the algebraic signs of the first order terms in eqs. (41) - (43) must be analyzed in order to determine the effects of truncation error terms in the kinetic energy calculation on the accuracy of the internal energy calculation. In regions of large gradients, the magnitude of these truncation error terms can be large because of their quadratic dependence on the first spatial derivatives. Since limitations on running time and machine storage necessitate fairly coarse computing meshes for two-dimensional simulations, the truncation errors related to the finite size of the mesh cell are more likely to be important than those related to the time step. Thus, the $O(\Delta x)$ and $O(\Delta y)$ terms in eq. (43) may dominate the truncation error. We shall see that this is the case in shaped charge calculations.

The inclusion of the truncation error terms in the kinetic energy calculation alters not only the computed values of the kinetic energy of a cell at each cycle but also the values of the internal energy. The coefficients of the Δt terms in eqs. (31) and (32) are positive and increase the kinetic energy. For equal spatial meshes ($\Delta x = \Delta y$), the entire first order term in the TPHASE calculation is negative for Courant numbers less than a half and decreases the kinetic energy. The effect of truncation error terms on the internal energy is reversed because of eq. (5). The SPHASE and HPHASE terms decrease the internal energy and the TPHASE increases it. Thus, these terms can be interpreted as a transfer mechanism which is not modeled by the governing equations and which converts internal energy into kinetic energy and kinetic energy into internal energy. Consider, for example, the one dimensional first order energy approximation in TPHASE for motion in the x-direction. The only first order term that the internal energy calculation includes is the positive term:

$$\frac{\rho_{i-1}\,\bar{u}^2}{2\rho^{n+1}}\,(\Delta x - \bar{u}^r\Delta t)\left(\frac{\bar{u} - \bar{u}_{i-1,j}}{\Delta x}\right)^2 . \tag{45}$$

Expanding expression (45) in a Taylor series about the cell center and the n^{th} time level, we obtain

$$(\lambda - \lambda')\left[\frac{\partial u}{\partial x}\right]^2 \tag{46}$$

to the lowest order, where $\lambda = 0.5\rho u\Delta x$ and $\lambda' = +0.5\rho u^2\Delta t$. If $(\lambda - \lambda')$ were the coefficient of viscosity, then expression (46) would be identical to the viscosity term in the one-dimensional internal energy equation for a viscous fluid. Thus, the energy transfer mechanism in this case could be defined as an explicit artificial viscosity term, since it is explicitly included in the difference equation much like the implementation of the von Neumann and Richtmyer artificial dissipation scheme.

Evans and Harlow[3] identified the term corresponding to $\lambda(\partial u/\partial x)^2$ in their one-dimensional analysis of the original PIC code. The term $\lambda'(\partial u/\partial x)^2$ is not included in their analysis, since they did not include the effect of time differencing. From expression (46), we see that the time discretization decreases the amount of kinetic energy converted to internal energy in TPHASE. This explicit type of artificial viscosity is confined only to the TPHASE energy calculation and is, in addition to the implicit artificial viscosity[6] (that type of artificial viscosity deduced from the neglected truncation error terms within an algorithm), already inherent in a first order algorithm.

IV. THE MODIFIED HELP CODE

We have shown that the terms of the order of the truncation error which are included in the kinetic energy calculation decrease the accuracy of the internal energy calculation under certain circumstances. To determine the effects of omitting these terms in such a calculation, the HELP code was modified to allow a kinetic energy calculation which did not include the first order terms in eqs. (31) - (33). Consequently, the kinetic energy was not computed by the updated mass and momentum values but was considered a separate dependent variable. This kinetic energy for both pure and mixed cells was updated according to a direct finite differencing of eq. (28) in a manner consistent with the other approximations and was stored in an array. The array TKEG contains the cell centered specific kinetic energy and the array TKEGM contains the specific kinetic energy of each material in an interface cell. By implementing such a scheme, the algorithm still numerically conserves mass, momentum and specific total energy as before but now possesses a new discrete dependent variable, the specific kinetic energy, and another finite difference equation. However, the modified version required slightly less computing time than the original version, since all the quantities needed to compute a new kinetic energy value are already available from the mass and momentum calculations and future references to the kinetic energy are simply retrievals. Throughout the modified algorithm references to the specific kinetic energy are always to the arrays TKEG and TKEGM and never to the quantity $0.5\ (u^2 + v^2)$. Although other formulations are possible, the present one calculates the specific kinetic energy in the desired manner (hence, the internal energy) and is relatively easy to implement in the existing HELP code.

Since an accurate calculation of the specific internal energy is the ultimate goal, a natural alternative to the 1975 HELP algorithm is the

6. Roache, P. J., Computational Fluid Dynamics, Chapter V, Hermosa, Albuquerque, 1976.

direct calculation of the specific internal energy in every phase. This type of algorithm deletes the truncation error terms in the internal error calculation. In several examples (shaped charge simulations were not included), Karpp[7] obtained significantly better internal energy values with this approach. A closely related algorithm is the 1971 version of HELP.[8] This version directly solves for the specific internal energy in the SPHASE and HPHASE portions of the algorithm but transported the specific total energy in TPHASE. A stated reason (see Ref. 1) for the current total energy version of HELP was the problems rising from the internal energy calculation in HPHASE. The two pass energy calculation in HPHASE caused inaccurate definitions of pressure and velocities near free surfaces and, consequently, the inclusion of the GLUE subroutine to rectify them. The GLUE subroutine was not totally satisfactory. The desire to avoid these past difficulties compelled us away from an internal energy formulation and to the retention of the total energy formulation.

The modifications listed below apply to the version of HELP described in Ref. 1. This original formulation is available on the BRL CDC 7600 under the permanent file name BRLHELP, CY = 14. The permanent file identification is ID = CMCHYDRO. The modification deck is listed in Appendix A. It is in CDC UPDATE[9] format and contains comment cards in order to explain each particular change. The modified version of HELP is available on the BRL CDC 7600 under the permanent file name BRLHELP, CY = 15. The permanent file identification is ID = CMCHYDRO.

In addition to the changes in the common deck, HELPCOM, the modifications affect 15 of the 57 subprograms in HELP: namely, SPHASE, HPHASE, TPHASE, EDIT, EQST, INPUT, SETUP, SETUPA, FILGRD, FLGSET, RNDOFF, NEWMIX, NEWFLG, ENCHCK, and UVMOD. The modifications incorporated into HELP enables one to run simulations involving all the options of HELP described in Ref. 1 except the penetration and rezone packages. The modifications have not been included in any of the plugging routines: PLGADD, PLGALF, PLGGEN, PLGMAS, PLGTCR, PLGVOL, PLUGUV, PTSAV,

7. Karpp, R. R. and Soldstein, S., "Modifications to the Hydrodynamic Computer Code HELP," Los Alamos Scientific Laboratory Summary Report R199, M-4-1596, December 1977.

8. Hageman, L. J. and Walsh, J. M., "HELP, A Multi-Material Eulerian Program for Compressible Fluid and Elastic-Plastic Flows in Two Space Dimensions and Time, Vol. I, Ballistic Research Laboratory Contract Report NO. 39, May 1971. (AD #726459)

9. Control Data Corporation, "UPDATE Reference Manual," Control Data Corporation Manual 60-449900, 1975.

or in the REZONE subroutine. However, a rezoning deck[10] which is used in conjunction with the REZONE subroutine was obtained. Both the deck and subroutine were modified to allow a limited rezone capability in the modified formulation. The restrictions on this rezone package are: i) the rezone package must be user-activated, ii) the computational grid can be extended only in the axial direction, and iii) the last row of computation cells (J = JMAX) must contain void. The rezone package combines cells as described in the HELP manual. The rezone deck (IDENTs REZJAS and CHREZ) and the modifications (INDENT CORREZ) are listed in Appendix B in CDC UPDATE format.

The modifications are implemented in such a way as to retain the total energy conservation within the computational grid. At the end of 859 cycles (t = 16 μs) in the 43 mm shaped charge calculation, presented in Section VI, the maximum relative error between the theoretical total energy and the actual total energy within the grid is 1.09×10^{-9}. For this calculation, the modifications increased the storage requirements by only 6% and decreased the running time by approximately 2%.

Finally, we note that another correction set is listed in Appendix A under the IDENT CORMAP. This enables the MAPS subroutine to indicate small magnitude negative values in the MAPS output. Prior to this correction, a single dash was used as a symbol for both positive and negative ranges of a variable's value. With this correction a single dash represents positive values and a double dash negative values.

V. MESH REFINEMENT STUDY FOR A WEDGE IMPACT CALCULATION

Since the study of the internal energy problem is based on a truncation error analysis, a mesh refinement study is appropriate to the investigation of the effects of the truncation error terms on the accuracy of the computed specific internal energies. Because of the complexity of a full shaped charge simulation, a related model problem[11] is simulated in the mesh refinement study. An observer stationed at the stagnation point in Fig. 7b (page 37) would find the uncollapsed liner moving towards him and separating into two parts (the slug and jet). Consequently, a 20 mm wide copper wedge traveling at 2 km/s was simulated as it impinged on a perfectly reflective wall at 30° of obliquity. The wedge collapse was modeled with slab symmetry. The material constants for the copper are CZERO = 0.235 GPa, RMU = 45.50 GPa, STK1 = 6.95 GPa,

10. Lacetera, J. M., USA Ballistic Research Laboratory, Private Communication, April 1978.

11. Birkhoff, G., et al., "Explosives with Lined Cavities," Journal of Applied Physics 19, 563-582, 1948.

STK2 = 5.5 GPa, STEZ = 0.53 MJ/kg and AMDM = 0.9785. See the HELP manual[1] for the definition of the above constants. The initial density of the copper is 8.9×10^3 kg/m^3. We note that the initial pressure and specific internal energies are zero, since the code computes the overpressures and specific internal energies above the initial state. Consequently, throughout this report, the values of the specific internal energy are relative to the initial reference value and are not the absolute values. The material surrounding the wedge is void. A single pass through SPHASE was used. The Tillotson equation of state[12] for copper was used. The coarse computational mesh was 30 by 100 cells ($\Delta x = \Delta y = 1$ mm) and the fine mesh was 60 by 200 cells ($\Delta x = \Delta y = 0.5$ mm). Both the original and modified version of the HELP code were run on a CDC 7600.

The results at 10μs after the wedge first impacts the wall are shown in Figs. 4-6. Besides the specific internal energy, two other important quantities, the relative axial velocity (relative to the end of the slug portion) and density, are compared along the wall in the slug, stagnation and jet regions. Qualitatively, the entire compression and relative axial velocity curves and the slug portion of the specific internal energy curve are similar among the mesh variations and version changes. However, the qualitative behavior of the jet's specific internal energy markedly differs between the two versions for either mesh. This is due to the increased gradients within the jet portion which can drastically increase the magnitude of the truncation error terms from the kinetic energy calculation, and thus, the truncation error. Quantitative comparisons were made at three positions in Figs. 4-6: the slug end, the stagnation point and the jet end. The symbol ↓ denotes the stagnation point (the cell along the wall with the largest pressure. While the total deviation among the relative axial velocity and compression curves from the largest computed value at the three stations was less than 7% (except for 9.9% in the compression at the jet's end), the total deviation of the specific internal energy curve was 82.1%, 26.4% and 63% at the jet, stagnation and slug, respectively. The tremendous increase in the total deviation of the specific internal energy curve is due to the first order terms included in the calculation of the kinetic energy. In fact, the deviation of the coarse mesh specific internal results from the fine mesh results, decreased by over 62% from the original version to the modified version. Consequently, one obtains much less variation in the specific internal energy values as one converges to the solution through a mesh refinement with the modified version. Fig. 6 suggests that the specific internal energy values which are computed by the modified version and with the coarse mesh provide a better approximation to the exact values than those values computed by the original version with the fine

12. Tillotson, J. H., "Metallic Equation of State for Hypervelocity Impact," General Atomic Report No. GA-3216, July 1962.

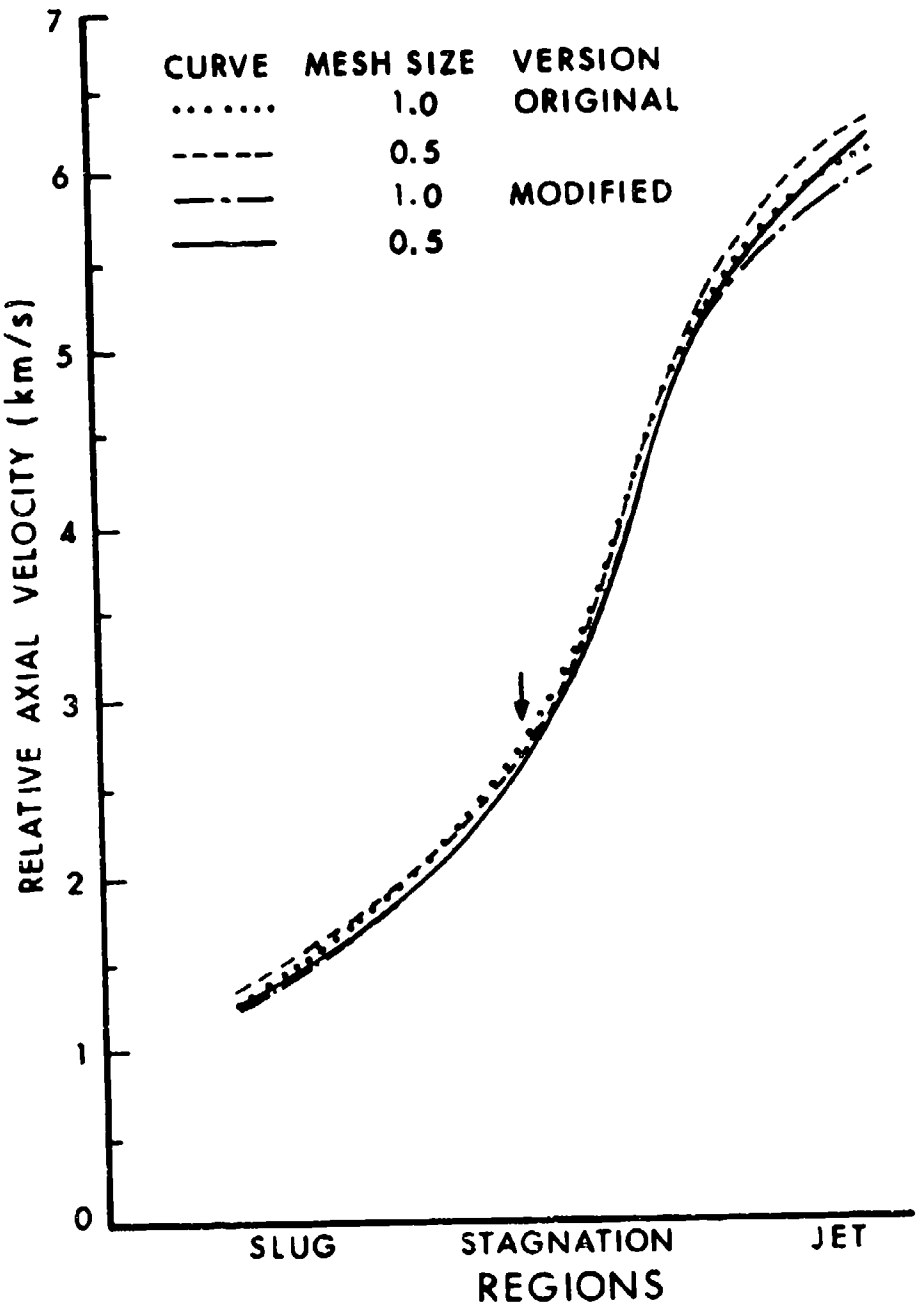

Figure 4. Spatial Profiles of the Relative Axial Velocity at 10μs Along the Wall for a Copper Wedge Impact Calculation

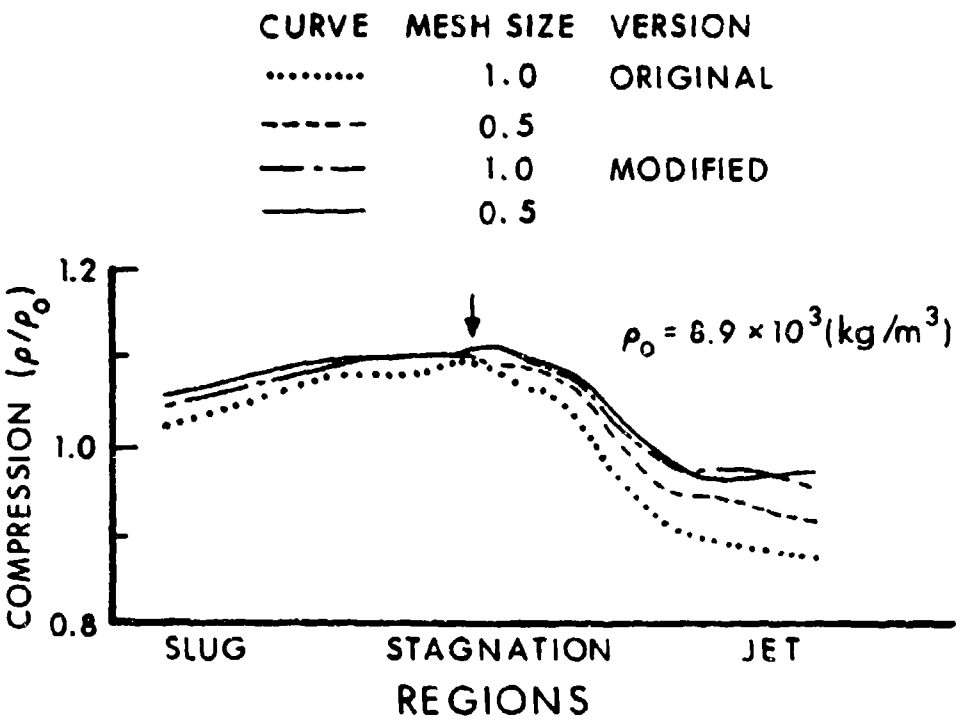

Figure 5. Spatial Profiles of the Compression at 10μs Along the Wall for a Copper Wedge Impact Calculation

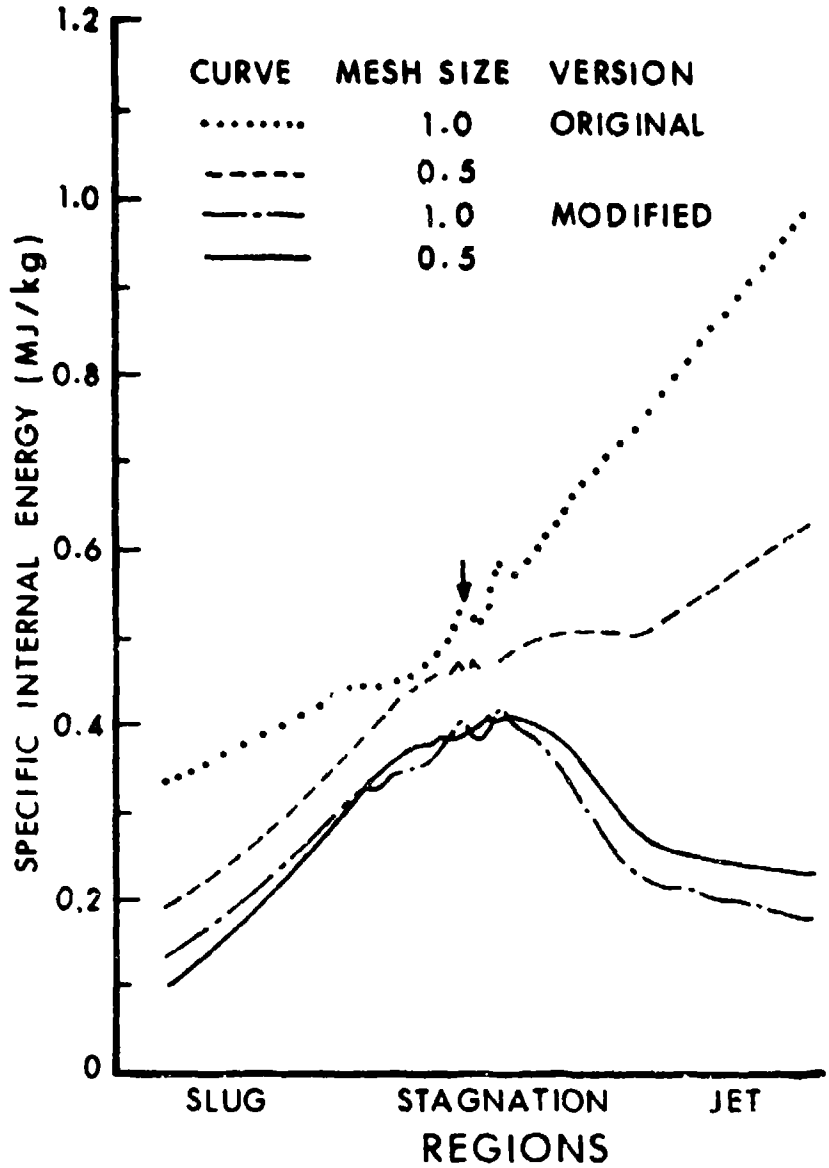

Figure 6. Spatial Profiles of the Specific Internal Energy at 10μs Along the Wall for a Copper Wedge Impact Calculation

mesh. This trend is also present in the compression curve. The results of Fig. 6 also show that for this type of problem, the truncation error terms in the kinetic energy calculation associated with TPHASE (Courant number of 0.4 is used) dominate those associated with SPHASE and HPHASE and cause the specific internal energy to be increased.

VI. THE COMPARISON OF THE MODIFIED AND ORIGINAL FORMULATIONS USING A 43MM CONICAL SHAPED CHARGE SIMULATION

We will consider the 43mm conical shaped-charge which is unconfined and has a rounded apex. See Fig. 7a. The actual warhead is obtained by rotating Fig. 7a about the axis of symmetry. The explosive is detonated and the detonation wave collapses the conical liner towards the axis of symmetry with a varying velocity. Sixteen microseconds after detonation, the liner consists of three parts (Fig. 7b): The uncollapsed liner, the low velocity large mass slug and the high velocity small mass jet. By performing a Galilean transformation at the point where an original ring of liner impinges on the axis of symmetry, a stagnation point in the flow can be shown to exist. This stagnation point divides the collapsed liner into the slug and jet. It is the jet which pierces the armor and is of prime concern to the shaped charge designer. By assuming that the liner can be modeled as an incompressible material under typical loading conditions, several researchers[11,13,14] have developed one-dimensional analytical or simple numerical models to determine the velocity field. However, when two-dimensional axisymmetric geometry, compressibility, strength, and thermodynamic effects are included, a full numerical simulation is necessary. The liner collapse and early jet formation of this shaped charge was simulated using the BRLSC[15] code (the precursor of the 1975 HELP code) and the results compared to experiments in Ref. 16.

13. Pugh, E. M., Eichelberger, R. M., and Rostoker, N., "Theory of Jet Formation by Charge with Lined Conical Cavities," Journal of Applied Physics 19, 563-582, 1948.

14. Kiwan, A. R. and Wisniewski, H., "Theory and Computations of Collapse and Jet Velocities of Metallic Shaped Charge Liners," US Army Ballistic Research Laboratory Report No. 1620, 1972. (AD #907161L)

15. Gitting, M. L., "BRLSC: An Advanced Eulerian Code for Predicting Shaped Charges, Volume 1," US Army Ballistic Research Laboratories Contract Report No. 279, December 1975. (AD #A023962)

16. Harrison, J. T., "A Comparison Between the Equlerian Hydrodynamic Computer Code (BRLSC) and Experimental Collapse for a Shaped Charge Liner," US Army Ballistic Research Laboratory Memorandum Report No. ARBAL-MR-02841, June 1978. (AD #A059711)

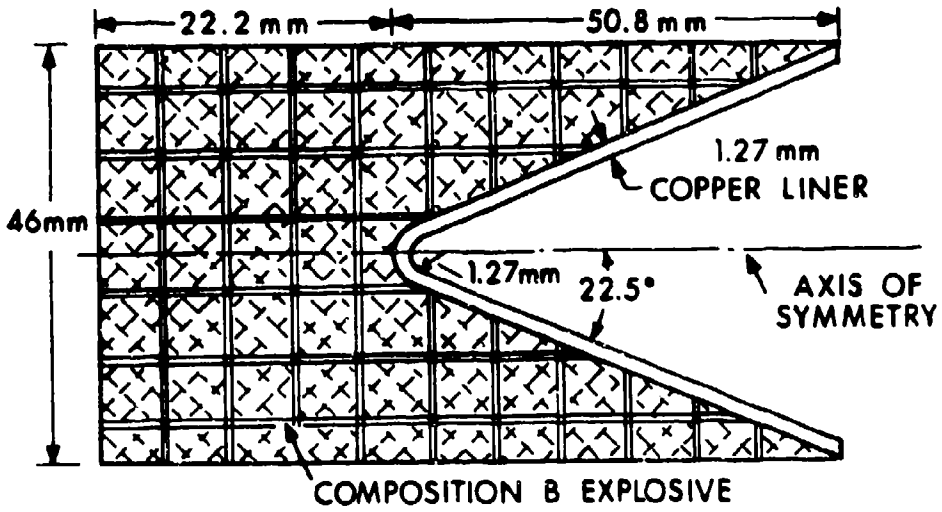

Figure 7a. Initial Conical Shaped Charge Configuration

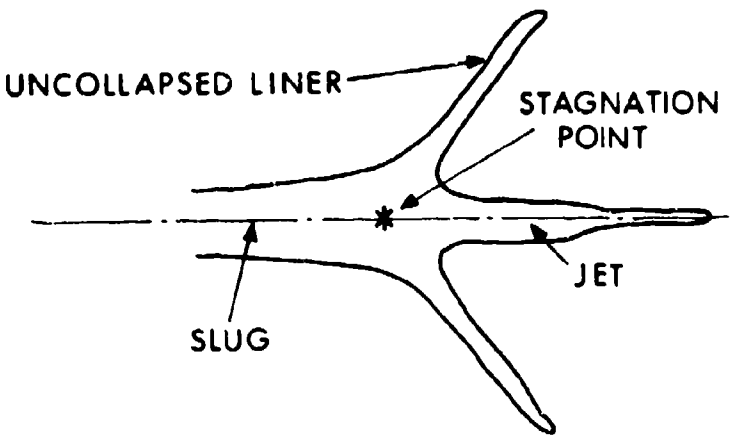

Figure 7b. Copper Configuration at 16μs for Conical Shaped Charge

Since the HELP code[1] is now generally used instead of the BRLSC code for shaped charge studies, we shall limit our discussion to the HELP's results. In order to further compare the original and modified versions of the HELP code, a conical shaped charge with a copper liner and Composition B explosive (Fig. 7a) is modeled in cylindrical coordinates and with identical material constants, initial conditions, code options and grid structure. The material constants for the copper are identical to those used in the copper wedge calculation. The slipline option is employed along the copper - Composition B interface. A void surrounds the entire warhead. The initial state is quiescent: all properties zero except the standard values of the densities (8.9×10^3 kg/m^3) for copper and 1.717×10^3 kg/m^3 for Composition B. The explosive is point detonated at the intersection of the axis of symmetry and the base of the Composition B. The computational mesh is 60 cells in the radial direction and 187 cells in the axial direction. The axial increment is $\Delta z = 0.52$ mm and the radial increment is $\Delta r = 0.52$ mm for the first 46 cells and slowly increases to 19.93 mm at the last radial cell. In both calculations the bottom boundary is transmittive. The strength option with a single pass is utilized (that is, the contribution of the stress deviator tensor is included). The Jones-Wilkins-Lee equation of state[17] for the explosive and the Tillotson equation of state[12] for the copper are used. The constants used in these equations of state are given in the HELP reference manaual[1]. Sample input-output for this shaped charge is given in Ref. 18. The calculations were performed on a CDC 7600.

Fig. 8 shows the specific kinetic energy along the axis of symmetry from the slug tail to the jet tip for both formulations at 16μs. The symbol ↓ denotes the stagnation point. This comparison shows that modified algorithm values are always larger than those of the original algorithm. Thus, the truncation error terms in the kinetic energy calculation associated with the spatial discretization dominate those associated with the temporal discretization. In fact, throughout the flow field, the original formulation gave smaller values of kinetic energy than the modified. Fig. 9 is the comparison of the specific internal energies along the axis of symmetry at 16μs. The modified code predicts up to 88% decrease in the specific internal energy values of the original code. Along the axis, the original formulation predicts a liquid-vapor slug and a liquid-vapor jet, whereas, the modified formulation predicts

17. Lee, E., Finger, M. and Collins, W., "JWL Equation of State Coefficients for High Explosives," Lawrence Livermore Laboratory Report No. UCID-16189, January 1973.

18. Lacetera, J., Jr., Lacetera, J. M. and Schmitt, J. A., "The BRL 7600 Version of the HELP Code," USA Ballistic Research Laboratory Report (in preparation).

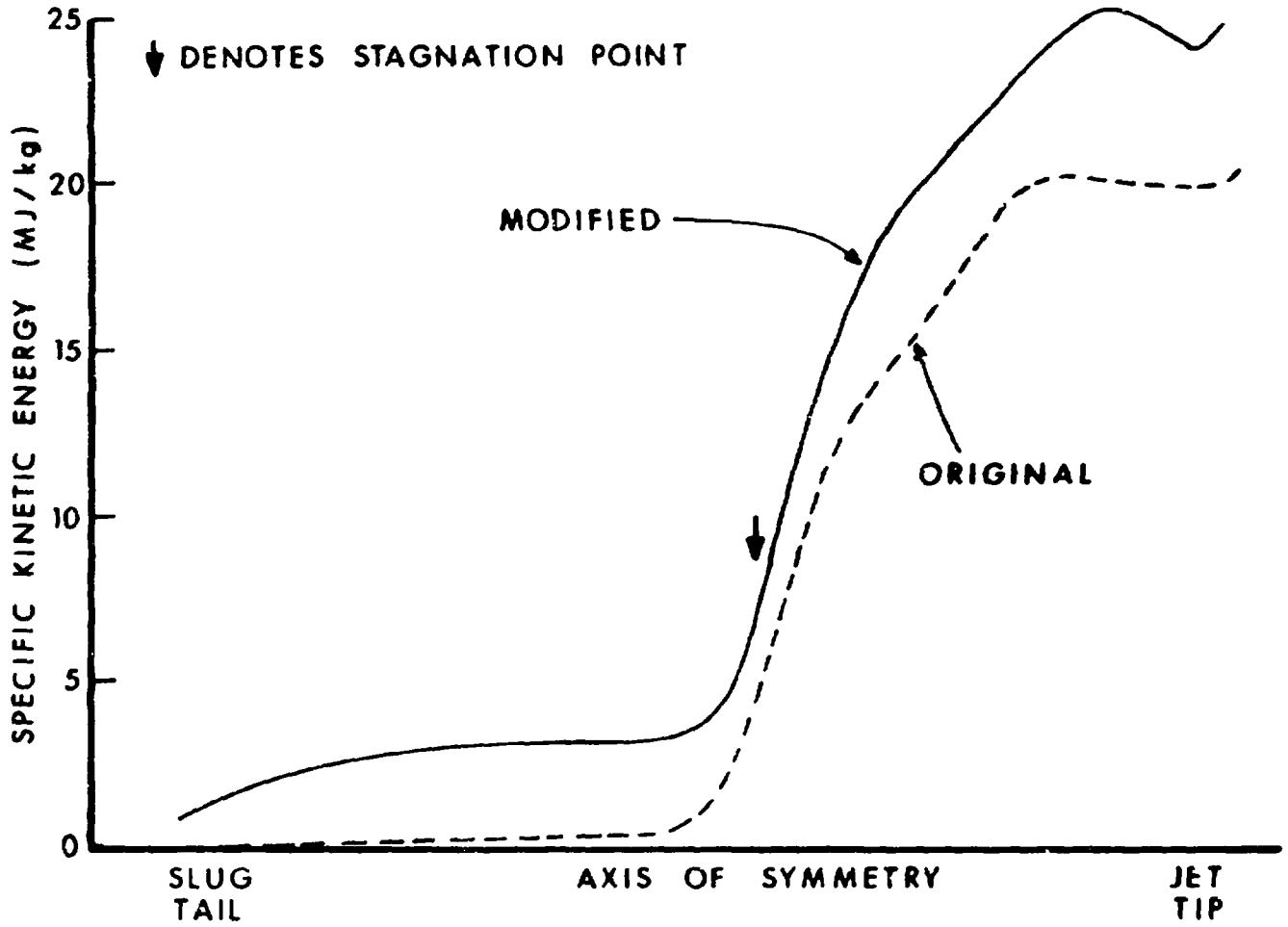

Figure 8. Comparison of the Specific Kinetic Energies Along the Axis of Symmetry at 16μs

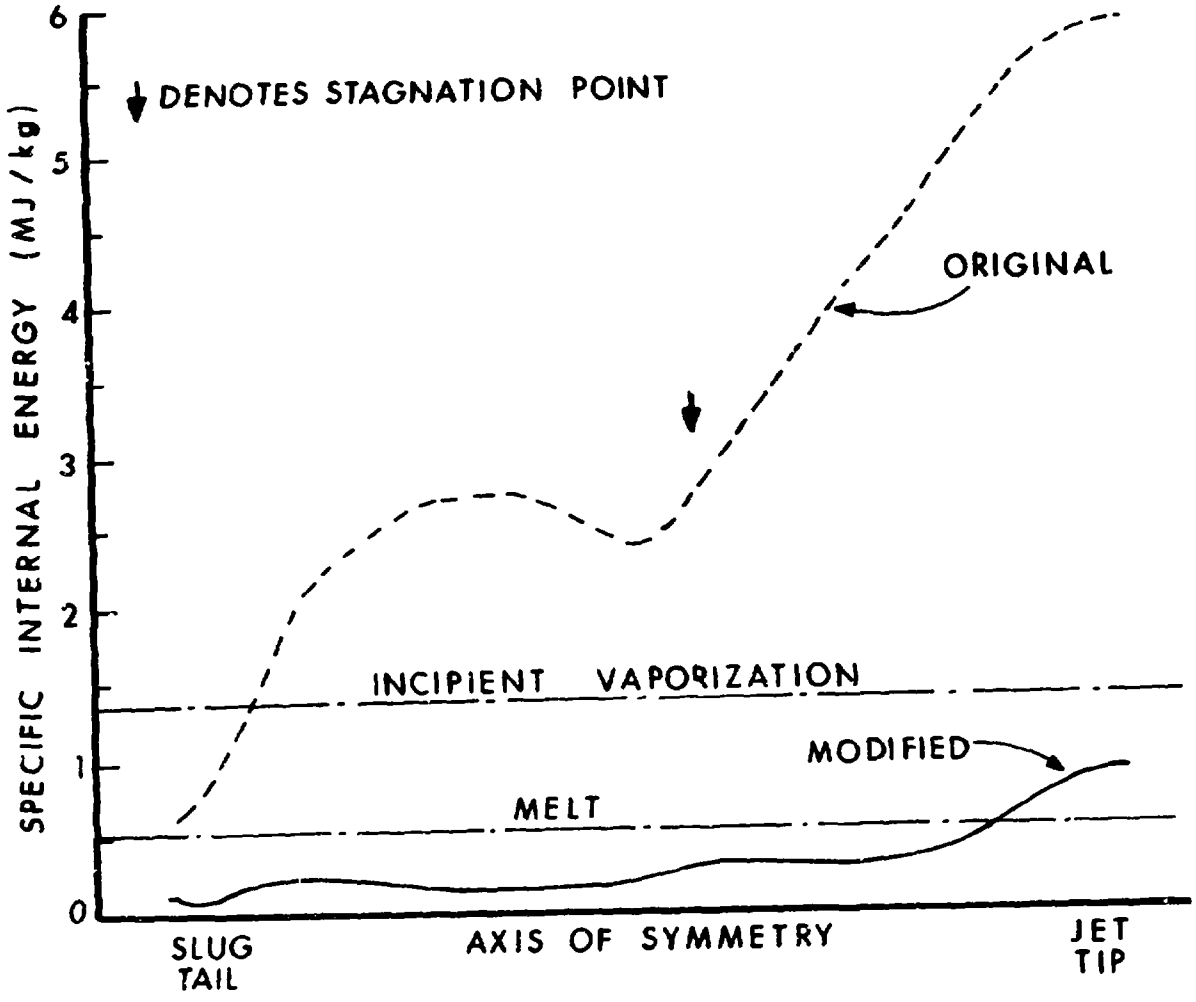

Figure 9. Comparison of the Specific Internal Energies Along the Axis of Symmetry at 16μs

a solid slug and a jet which remains a solid until near the tip region where it liquifies. We note that the BRLSC code results[16] indicate even a higher specific internal energy value than the HELP 1975 algorithm. The specific internal energy value corresponding to the melting point of copper 53 MJ/kg) is a material property input value. The specific internal energy value corresponding to the incipient vaporization point of copper (1.38 MJ/kg) is contained within the Tillotson equation of state. In the original formulation, the specific internal energy of each cell in the entire jet is well above the value corresponding to incipient vaporization at 16μs. Thus, the jet is characterized as a liquid-vapor jet. However, in the modified formulation, the specific internal energy of the same cells is generally below that for melt and a solid jet with several melted sections is predicted. See Fig. 10. Although no actual temperature measurements have been taken for this shaped charge, experimental evidence of Von Holle and Trimble[19] supports the conclusion that the copper jet is in the solid state. Thus, qualitative thermal agreement is achieved for the first time with the modified formulation. Fig. 11 illustrates the specific internal energy values generated by the modified formulation at various times along the axis of symmetry from just behind the stagnation point to the jet tip. The relative positions of the curves do not indicate their actual relative positions predicted by the code. The decrease in the specific internal energy values in the jet as a function of time is not constant and become less as time increases. The proportion of the computational cells within the jet with a specific internal energy value higher than that of melt decreases from 1.00 to 0.76 to 0.32 to 0.24 as time increases from 8 to 12 to 16 to 18.5μs, respectively.

Major differences in the internal energy illustrated in Fig. 9 will drastically affect the material properties of the slug and jet. An investigation into the copper's strength, ductibility and cohesion cannot be computationally investigated with the original version of HELP, since it predicts a liquid-vapor state for most of the copper in the slug and jet. In particular, when the specific internal energy of a cell is equal to or greater than that for melt, the stress components are equated to zero and the flow variables remain unchanged during SPHASE. Consequently, in the original formulation and for the 43mm conical shaped-charge problem, the inclusion of the strength option does not generate significantly different values of the flow variables. Since the values of the specific internal energy in the modified version are almost always below melt, the inclusion or exclusion of the SPHASE contribution is now primarily controlled by the tensile failure criterion. If the material density ρ is such that $\rho/\rho_o <$ AMDM (ρ_o = initial density), the material has failed and the SPHASE contribution is ignored.

19. Von Holle, W. G. and Trimble, J. J., "Shaped Charge Temperature Measurements," Proceeding of the Sixth Symposium on Detonation, San Diego, August 1976.

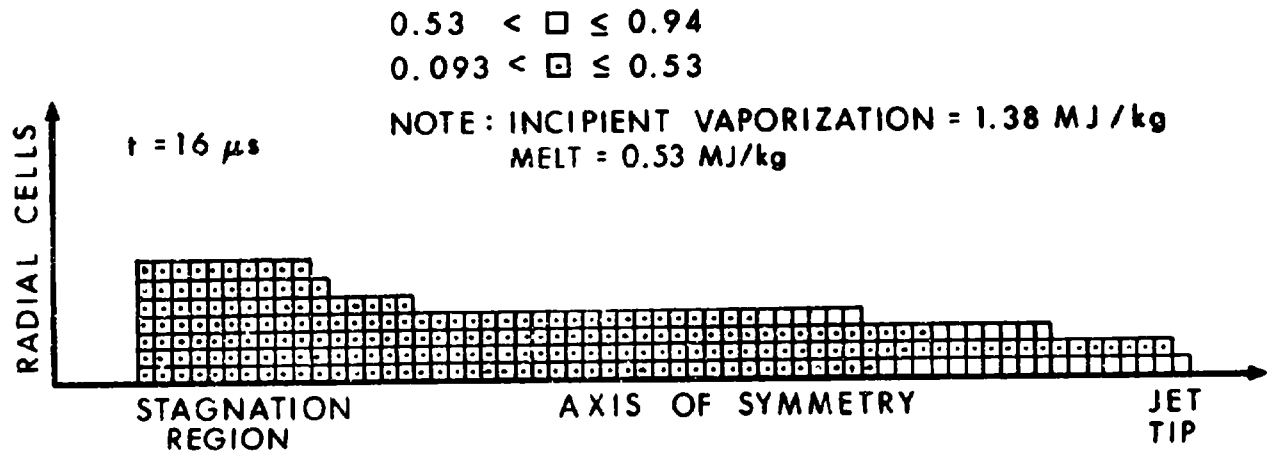

Figure 10. Cell-Centered Values of the Jet's Specific Internal Energy (MJ/kg) Computed by the Modified Formulation

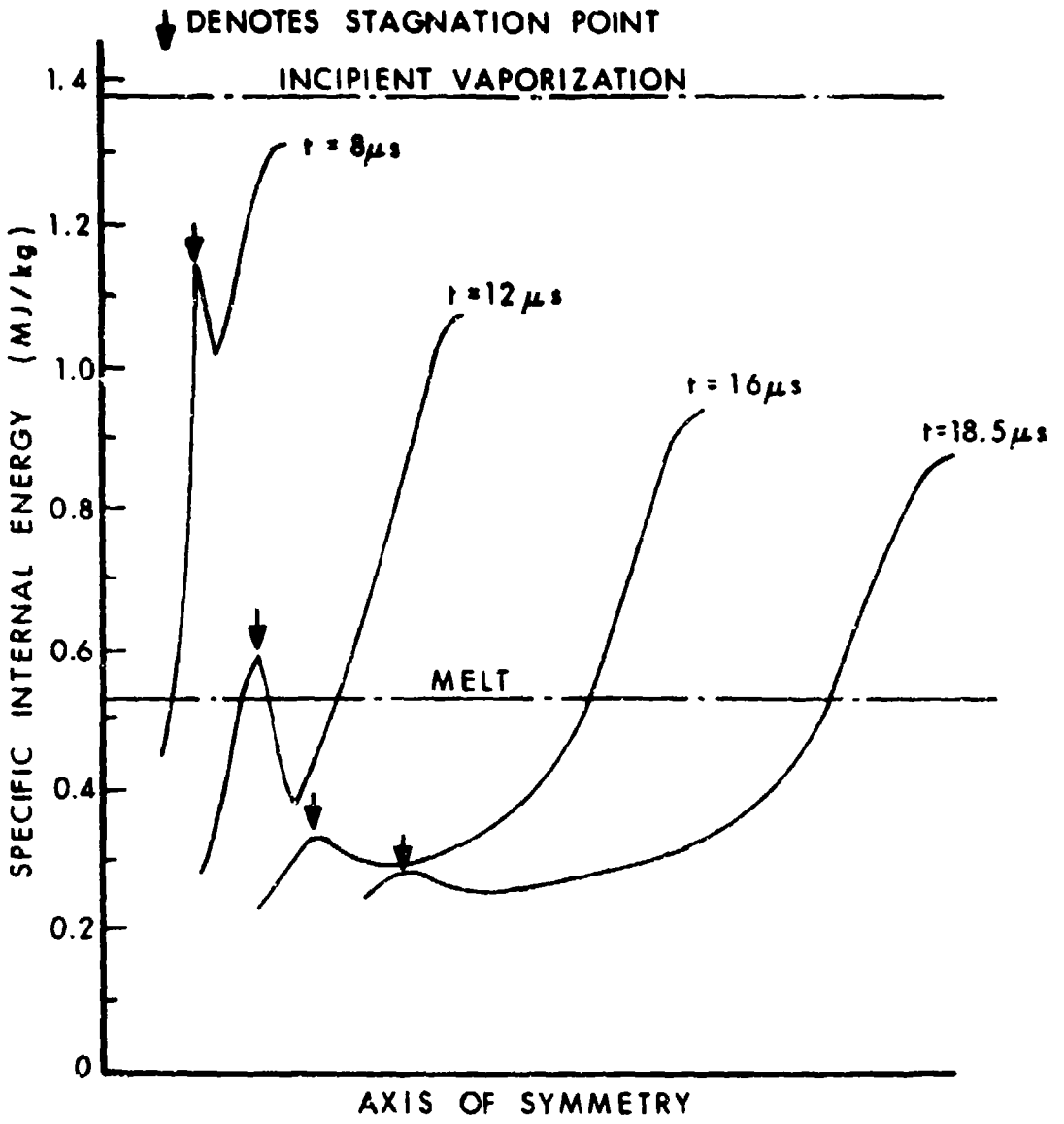

Figure 11. Modified Version's Specific Internal Energy Profiles from the Stagnation Region to the Jet Tip at Various Time

The parameter AMDM is a material strength input value. Hence, the effects of SPHASE on a conical shaped charge calculation are now dependent on an input value. A sensitivity study of the calculation on this parameter AMDM should be made with the modified formulation. However, such a comparison is not included in this report.

Comparisons of the pressures, velocities, specific total energies and densities between the two versions along the axis of symmetry at 16μs are shown in Figs. 12-17. Although significant differences in the above quantities are expected, especially within the jet, as the result of phase differences predicted by the codes (see Fig. 9), the discrepancies between the versions are not major, except for the density. The cause of the small discrepancies can be traced to the pressure calculation. The effect of the specific internal energy on the other computed quantities is controlled by the equation of state. In the original version, a predetermined upper bound on the specific internal energy is used in the equation of state for the liner material in an ad hoc manner. For shaped-charge calculations (code option NLINER $\neq$ 0), the maximum value of the specific internal energy utilized in the equation of state for the primary liner material is the incipient vaporization value. In our example, the largest specific internal energy value used in the pressure calculation of the original version is 1.38 MJ/kg, even though all the cells of the jet have values above 1.38 MJ/kg. In the modified version of HELP, the ad hoc usage of this upper bound is abandoned. Hence, the pressure and other variables are consistent with the actual computed value of the specific internal energy in the modified version.

The pressures are compared in Fig. 12. The graph corresponding to the values computed by the modified formulation show a more uniform decay to the initial pressure. The stagnation point overpressure of the modified version is 6% greater than that of the original version. The stagnation point occurs at the same position in both versions. The graphs of the pressure and of the radial velocity (Fig. 15) and the compression (Fig. 17) correlate well for the jet and slug's interior. Regions of high pressure correspond to large negative radial velocities and values of compression greater than one. The axial velocities of the two formulations (Fig. 13) are identical near the stagnation region. Both versions predict that the physical inverse velocity gradient is still slightly present near the jet tip. The larger values of the axial velocity cause the slightly longer jets of the original formulation (approximately two computational cells). The effect of the inverse velocity gradient on the kinetic energy can be seen in Fig. 8. As in Fig. 13, the gradient is larger in the modified version than in the original. The jet tip velocity values of the original formulation (Fig. 14) are somewhat larger for times greater than 5μs but the percentage difference is small--at 16μs, the difference is less than 2%. The relative jet tip (jet tip minus slug tail) velocity predicted by the modified version at 16μs is 6.023 km/s. This value is 7.9% lower than the experimental value cited in Ref. 16. The radial velocities are compared

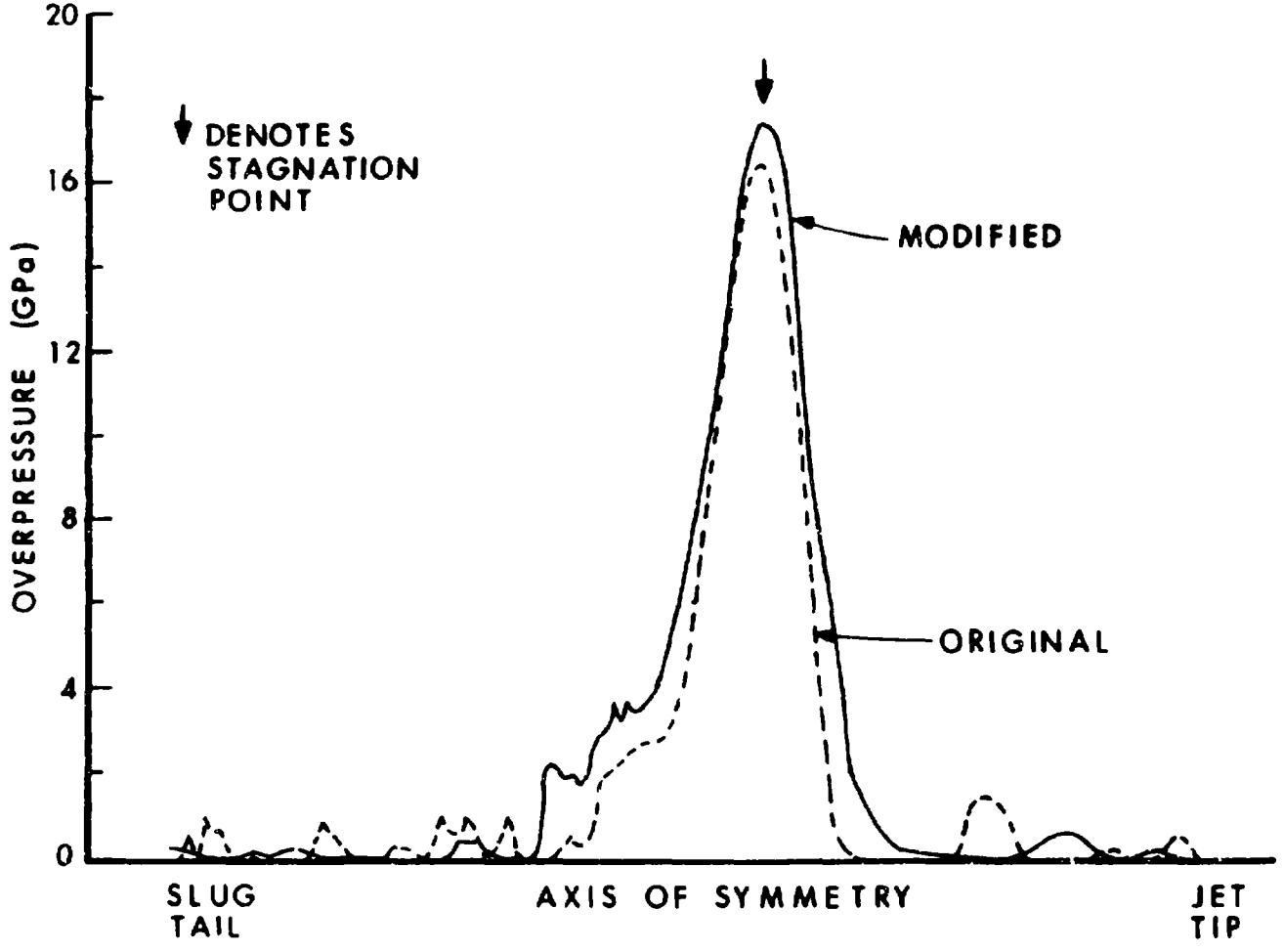

Figure 12. Comparison of the Pressures Along the Axis of Symmetry at 16μs

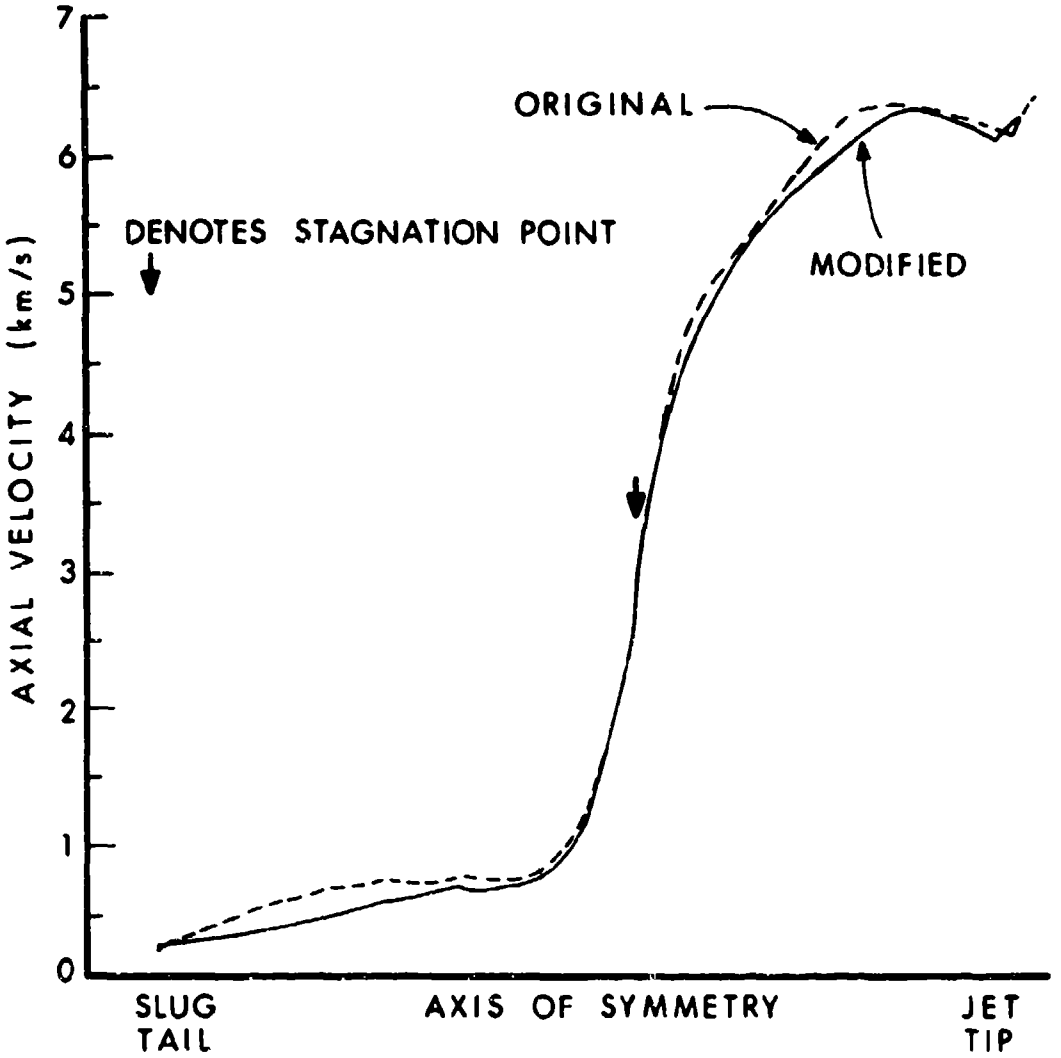

Figure 13. Comparison of the Axial Velocities Along the Axis of Symmetry at 16μs

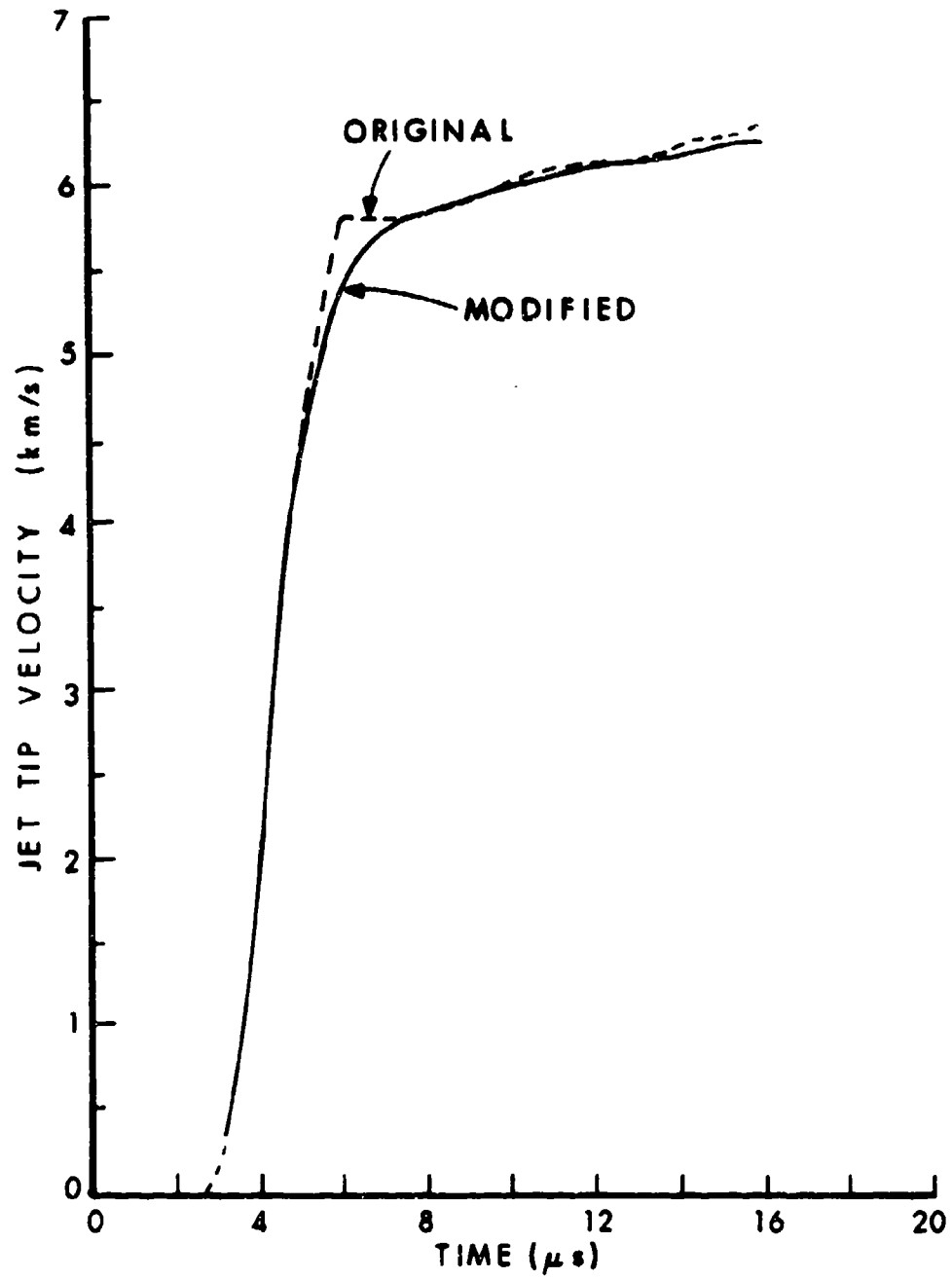

Figure 14. Comparison of the Jet Tip Velocity-Time Histories

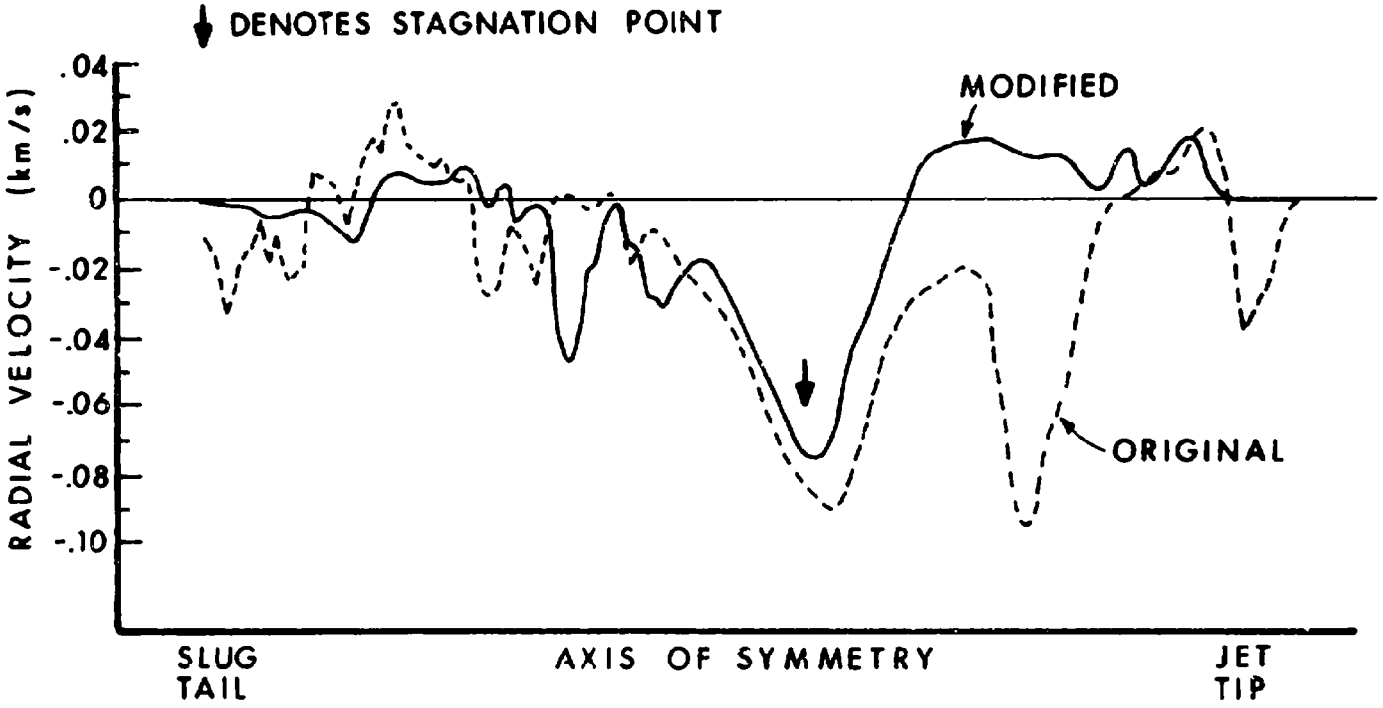

Figure 15. Comparison of the Radial Velocities Along the Axis of Symmetry at 16μs

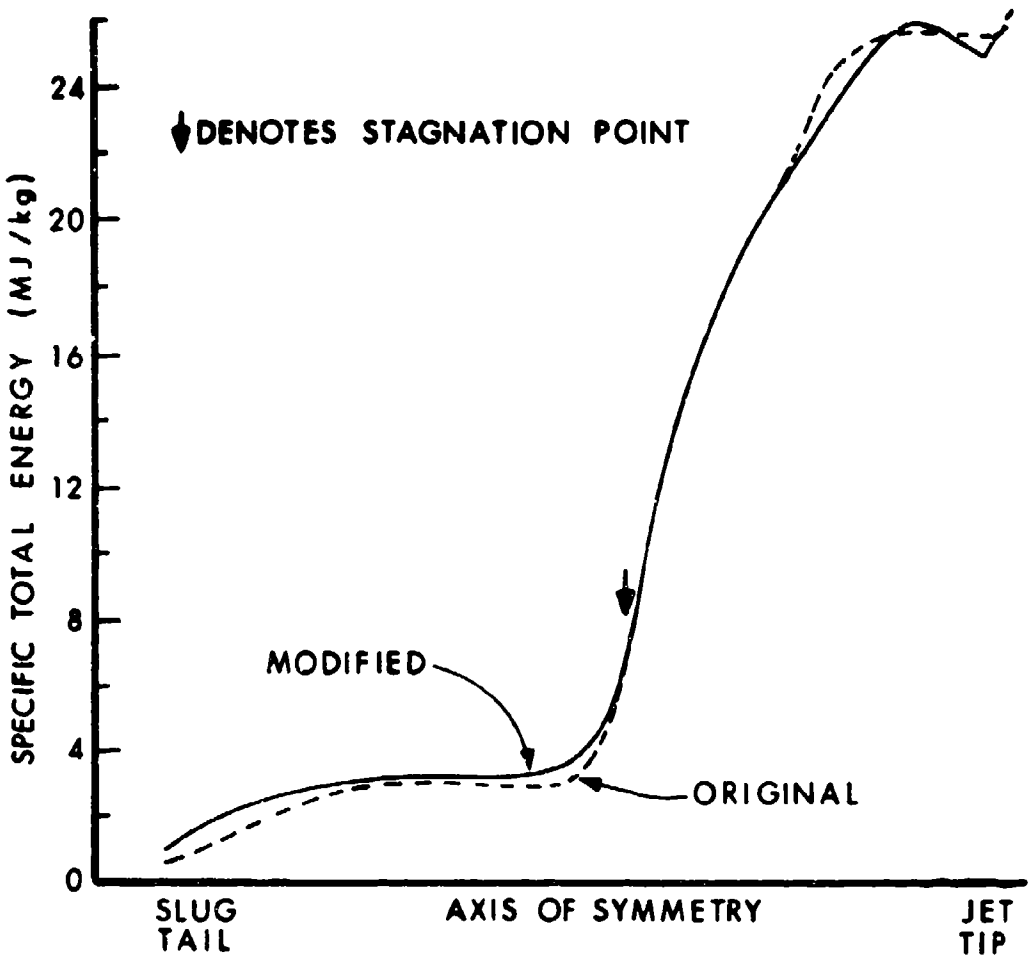

Figure 16. Comparison of the Specific Total Energies Along the Axis of Symmetry at 16μs

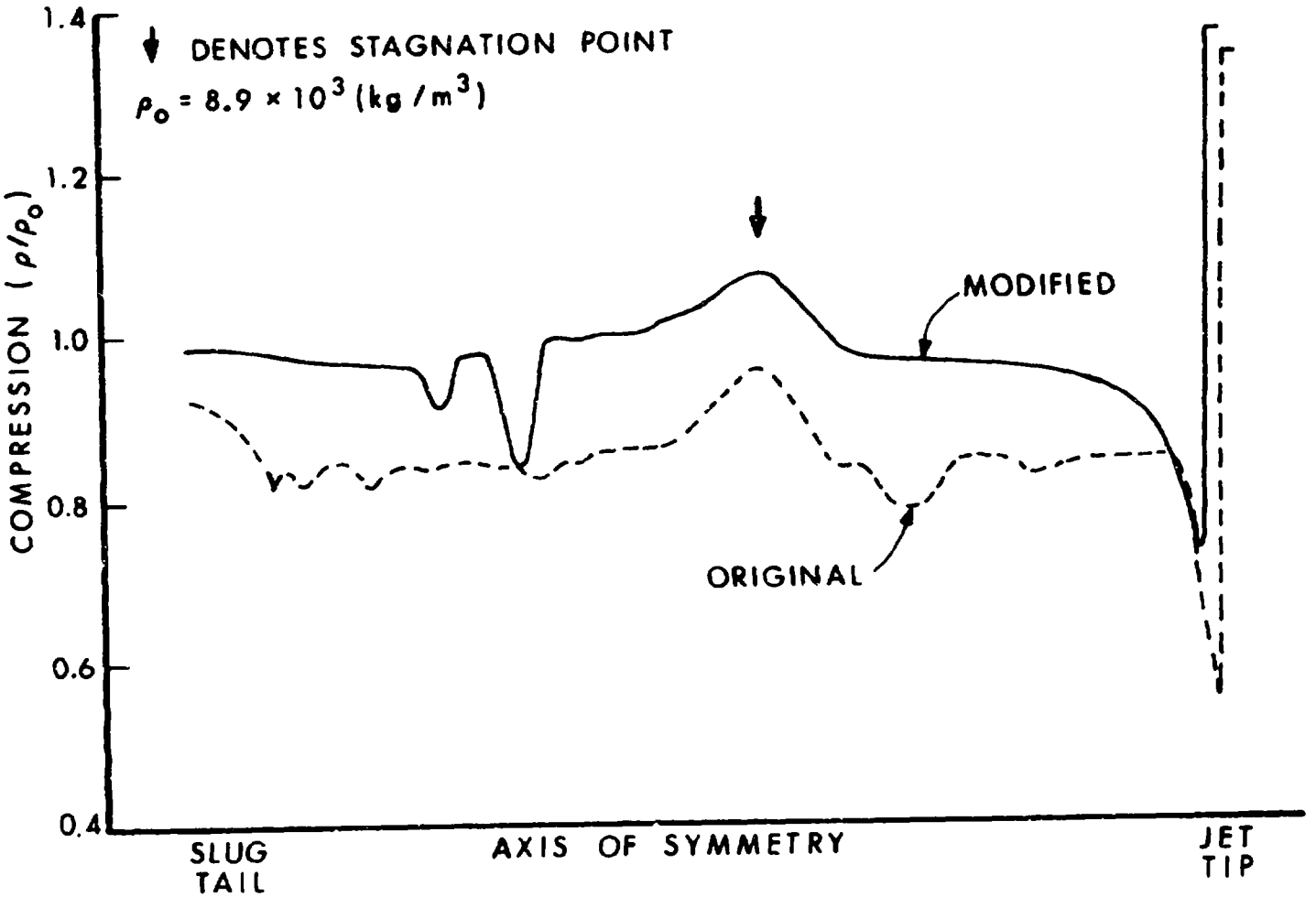

Figure 17. Comparison of the Compressions Along the Axis of Symmetry at 16μs

in Fig. 15. Since the radial velocity is modified so that the jet material at zero overpressure will not expand radially (zero radial velocities are imposed), an accurate assessment of this quantity is difficult away from the stagnation region. However, in the modified formulation the negative radial velocities, which cause a compression of the copper at the axis of symmetry, correlate well with the nonzero pressure values in Fig. 12. In the original formulation, this type of correspondence is not as well correlated. The specific total energies of the two versions are compared in Fig. 16. The effect of the small inverse velocity gradient seen in Figs. 8 and 13 is again reflected in the graph of the specific total energies. Fig. 17 shows a comparison of the compression (ρ/ρ_0) values. Throughout most of the slug and jet, the density values of the modified code are approximately 10% greater than the original. The density discontinuity which appears near the jet tip in both formulations could be numerically caused. See Section VII. The magnitude of the jet tip's discontinuity is larger in the original version and so is its associated undershot. Before decreasing to the final undershot value in the modified version, the jet's density is approximately 95% of the initial density of the liner. No density measurements have been experimentally determined for the 43mm copper shaped charge. However, experimental results for a 36mm copper shaped charge[20] predict the density variation of the unbroken jet to be from 90% to 81% of the initial liner density. Although the original version seems to be in better agreement with Jamet's results than the modified version, a HELP simulation of the actual experiment with identical explosives and configurations would have to be completed in order to accurately ascertain which version possessed the better correspondence. In the stagnation region, the modified formulation gives improved values-compression ($\rho > \rho_0$) of the copper. The sudden density decreases in the slug region predicted by the modified version can be correlated to the sudden pressure decreases. See Fig. 12.

Negative specific internal energy values are computed by both formulations of the HELP code in the uncollapsed liner and along the interface between the slug and the explosive. However, in the modified formulation the number and magnitude of the negative internal energy values increase. This is consistent, since the original formulation added the positive values of the truncation error terms in the specific kinetic energy calculation to the specific internal energy. See the discussion of Fig. 8. The computed specific internal energy value is the value over the initial specific internal energy. Consequently, the actual internal energy of a material in a computational cell may still be positive even though the computed value is negative. Nonetheless, in a total energy formulation, the computed negative specific internal energy values are

20. Jamet, F., "Measure de la densite d'un jet de charge creuse en curvre par radiographic-eclair," Saint-Louis, Rapport-Bericht R 101/76, 9.1.1976.

a consequence of the computed kinetic energy being greater than the computed total energy. The numerical source of this situation in the HELP code must be identified and corrected before any simulation can be completely satisfactory.

VII. TEMPERATURE CALCULATIONS FOR THE 43MM CONICAL SHAPED CHARGE

It is not the purpose of this section to give a definitive statement on the temperature distribution within the jet for a 43mm shaped change but rather to identify the current problems in an accurate temperature calculation and to present a first attempt in computing a temperature profile. The computed profiles do agree qualitatively with experimental evidence[19].

Since the Tillotson equation of state used in HELP does not compute temperature values, the temperature routine from the HULL code[21] was utilized. The HULL's temperature routine is a temperature fit which uses data in Ref. 22 and requires values of the density and specific internal energy. The coding used in the HELP code is listed in Appendix C. This routine was chosen, since it is used for temperature measures in shaped charge simulations by the HULL code and it is accessible. However, the question of its applicability to simulations involving phase transitions (from solid, through melt, to liquid) is unanswered. A definite need does exist for a highly accurate copper equation of state (see Ref. 23). More sophisticated equation of states, such as the BRLGRAY[24] equation of state, could be used when they are incorporated in the HELP code.

Since the temperature depends explicitly on the density and specific internal energy, accurate values of these quantities are essential to a correct temperature calculation. For example, if the density value is

21. Klem, G. J., US Army Ballistic Research Laboratory, Private Communication, April 1978.

22. Thompson, S. L. and Lauson, H. S., "Improvements in the Chart D Radiation-Hydrodynamic Code, III: Revised Analytic Equation of State," Sandia Laboratories Report No. SC-RR-71-0714, March 1972.

23. Edwards, L. L. and Godfrey, C. S., "Computer Code Design of Shaped Charges," Lawrence Livermore Laboratory Report No. UCRL-52598, October 1978.

24. Wray, W. O. and Cecil, R. A., "Modified Gray: An Improved Three-Phase Equation of State for Metals," US Army Ballistic Research Laboratory Contract Report No. 299, April 1976. (AD #A025260)

9.8×10^3 kg/m^3 and specific internal energy value is 0.46667 MG/kg, then a 6.43% decrease in density and a 3.45% increase in the specific internal energy produces over a 15% change in the calculated HULL temperature value. Consider Table 1 which lists the jet's density for the modified version at 16μs within the computational cells from the jet tip to the stagnation region. The prefix M with a number indicates that it is a free surface cell (a mixed cell composed of void and copper). The striking feature of the array of numbers is that in a given column the density of every free surface cell is identical. This peculiarity results from the numerical algorithm in HELP (see subroutine NEWRHO) and is not necessarily a physical result. The same phenomenon occurs in both the original and modified formulations. Thus computed temperature value involving a free surface cell would be at best suspect. Consequently, a comparison with Von Holle and Trimbles' experimental jet skin temperature [25] will not be made. First, HELP's free surface density calculation must be analyzed and modified, if necessary.

With an awareness of the limitations discussed above, we now consider the temperature profile within the jet (pure cells only) with the HULL temperature routine. We note that the specific internal energy computed by the HELP code must be augmented by an initial value of 0.113335748 MG/kg (corresponds to a temperature of 287.87K at an initial pressure of 0.101325 MPa) to obtain the actual value of the copper's specific internal energy. Between 16 and 18.5μs, the jet is defined by at most three pure cells in the radial direction for a given axial position. Figs. 18 and 19 show the temperature profile at 16 and 18.5 μs, respectively, of pure cells within the jet at various radial positions. The radial distances 0.26 mm, 0.78 mm and 1.3 mm measure the length from the axis of symmetry to the center of the first, second and third radial cells, respectively.

The melting point of copper under the initial conditions is 1356.6K.[26] The code predicts non-ambient pressures in the jet along most of the axis of symmetry and ambient pressures in most of the second and third radial cells. Consequently, the r = 0.78 mm and r = 1.3 mm curves in both figures predict that the jet is in the solid state. Along the axis of symmetry one cannot determine the actual state of the copper without more precise thermodynamic data. Throughout most of the jet, the results of the modified HELP substantiates Von Holle and Trimble's conclusion[19] of a solid jet. Thus qualitative thermal agreement between experimental evidence and computer simulation is achieved

25. Von Holle, W. G. and Trimble, J. J., "Temperature Measurement of Copper and Eutectic Metal Shaped Charge Jets," US Army Ballistic Research Laboratory Report No. 2004, 1977. (AD #B021338L)

26. Stull, D. R. and Prophet, H., (project directors), JANAF Thermochemical Tables, 2d ed, June 1971.

Table 1. Density Variation Within the Jet at 16μs

Distance from Axis of Symmetry				
.26mm	.78mm	1.30mm	1.82mm	2.34mm
M 12.132				
M 12.132	M 8.9000			
6.7517	M 8.9000			
6.2893	M 8.9000			
6.8630	M 8.9000			
7.1872	M 8.9000			
7.5139	M 8.9000			
7.7672	M 8.9000			
7.9480	M 8.9000			
8.0471	M 8.9000	M 11.312		
8.0855	8.4719	M 11.312		
8.1110	8.4878	M 11.312		
8.1416	8.4871	M 11.312		
8.1748	8.4725	M 11.312		
8.2110	8.4431	M 11.312		
8.2516	8.4116	M 11.312		
8.2899	8.3869	M 11.312		
8.3201	8.3734	M 11.312		
8.3479	8.3634	M 11.312		
8.3787	8.3598	M 11.312		
8.4203	8.2745	M 11.312	M 9.5116	
8.4490	8.1465	5.6167	M 9.5116	
8.4415	7.9541	6.3971	M 9.5116	
8.4466	7.7437	7.2789	M 9.5116	
8.4523	7.5188	7.8684	M 9.5116	
8.4590	7.2879	8.2828	M 9.5116	
8.4672	7. 0657	8.5278	M 9.5116	
8.4826	6.8687	8.6512	M 9.5116	
8.4955	6.7251	8.6535	M 9.5116	
8.5033	6.6794	8.6595	M 9.5116	

Distance from Axis of Symmetry				
.26mm	.78mm	1.30mm	1.82mm	2.34mm
8.5098	6.7489	8.6662	M 9.5116	
8.5169	6.9168	8.6703	M 9.5116	
8.5242	7.1430	8.6714	M 9.5116	
8.5315	7.3787	8.6683	M 9.5116	
8.5384	7.5989	8.6639	M 9.5116	
8.5447	7.7892	8.6596	M 9.5116	
8.5503	7.9460	8.6555	M 9.5116	
8.5551	8.0763	8.6517	M 9.5116	
8.5592	8.1903	8.6476	M 9.5116	
8.5633	8.2976	8.6428	M 9.5116	
8.5682	8.4025	8.6379	M 9.5116	
8.5755	8.4998	8.6347	M 9.5116	
8.5862	8.5737	8.6345	M 9.5116	
8.6028	8.6112	8.6384	M 9.5116	
8.6258	8.6252	8.6484	M 9.5116	
8.6560	8.6424	8.6643	M 9.5116	
8.6986	8.6732	8.6847	M 9.5116	M 10.300
8.7595	8.7211	8.7095	8.1814	M 10.300
8.8457	8.7933	8.7783	8.7366	M 10.300
8.9525	8.8877	8.8633	8.7632	M 10.300
9.0733	8.9954	8.9840	8.8093	M 10.300
9.1999	9.1256	9.1073	8.9486	9.0024
9.3208	9.2644	9.2399	9.1501	9.1263
9.4284	9.3906	9.3741	9.3290	9.2913
9.5076	9.4807	9.4753	9.4459	9.4682
9.5560	9.5382	9.5370	9.5223	9.5073
9.5740	9.5614	9.5605	9.5528	9.5553

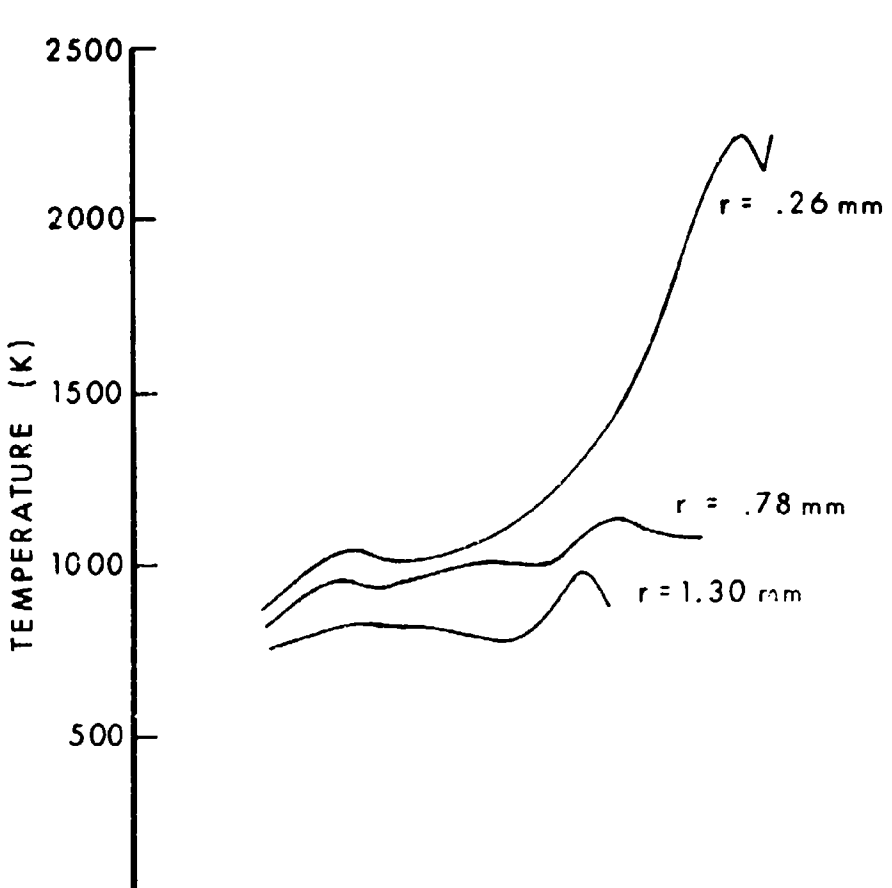

Figure 18. Variation of Jet's Temperature with Axial Distance at Various Distances from the Axis of Symmetry at 16μs

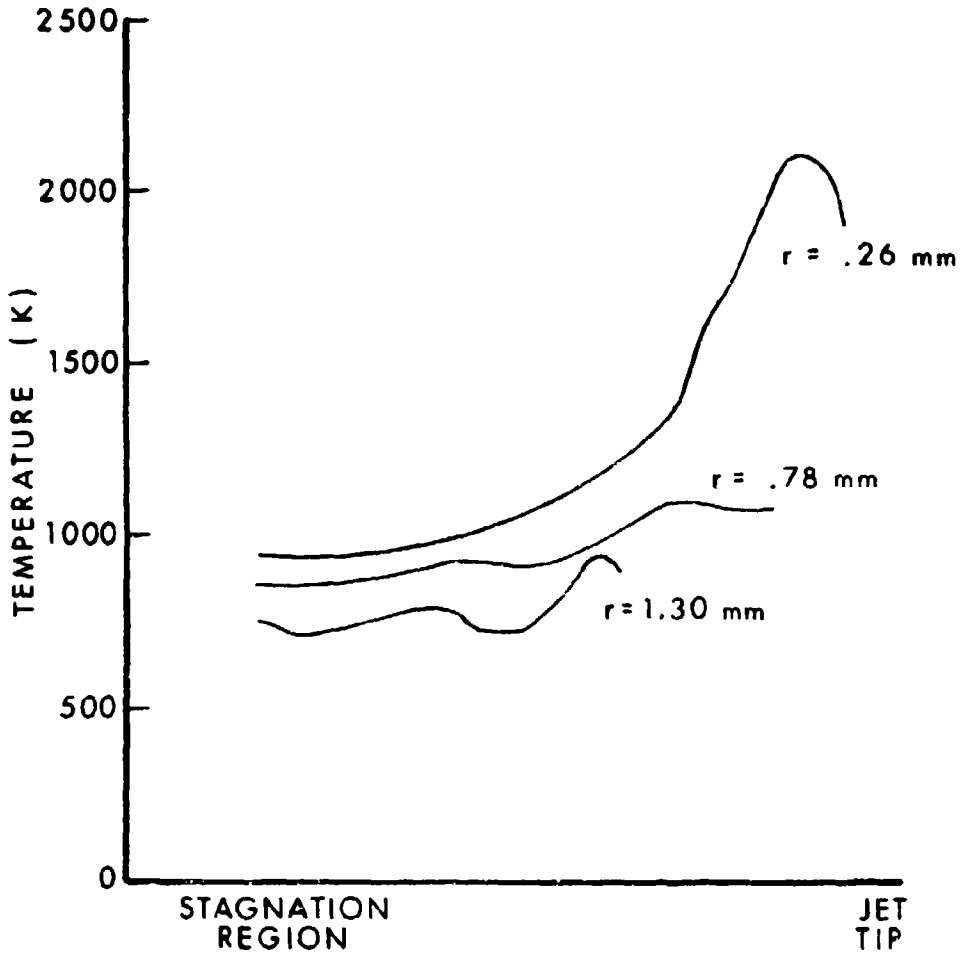

Figure 19. Variation of Jet's Temperature with Axial Distance at Various Distances from the Axis of Symmetry at 18.5us

for the first time. Finally, the temperature profiles in the jet decrease with time since the jet is expanding.

For comparison, the values of the density and specific internal energy from the original versions were used with the HULL temperature routine. The corresponding temperature values in almost every pure cell within the jet were greater than 3000K. At ambient conditions, the vaporization temperature of copper is 2848K.[26] These temperature results are larger than those implied by experimental evidence by at least a factor of two.

VIII. SUMMARY

We have shown by a truncation error analysis that terms of the order of the truncation error in the HELP algorithm are included in the kinetic energy calculation. In the original HELP code, the updated values of kinetic energy were computed as consequences of the updated mass and momentum values. This value is shown to deviate from that computed directly by a first order approximation of the kinetic energy equation by first order terms which depend quadratically on the spatial derivatives of the velocity, pressure, and elements of the deviator stress tensor. These truncation error terms can severely alter the related internal energy calculation. The effect of these truncation error terms from the kinetic energy calculation on the accuracy of the internal energy is problem-dependent and the criteria for such a determination is given in terms of the explicitly calculated truncation error terms for the specific internal energy. A method was suggested to avoid these terms within the confines of the basic HELP algorithm. Although in certain computations these truncation error terms may remain negligible, in others they can be significant and produce spurious results. A case in point has been cited and illustrated by applications to problems in warhead mechanics. A mesh refinement study for a copper wedge impacting a perfectly reflective wall was made. The results show tremendous deviations as the mesh size decreases in the internal energy values, while other quantities show relatively little deviations. In the modified formulation, significantly smaller deviations in the internal energy values and consequently, a more consistent deviation with the other quantities are observed. Drastic improvements in the internal energy values are also seen in conical shaped charge calculations. Temperature profiles of the jet's interior were computed using the temperature fit routine from the HULL code. When ambient pressures are computed by the code, the corresponding values of the temperature are between 700(K) and 1100(K) which are well below that for melted copper. Thus, qualitative thermal agreement is achieved for the first time between a HELP code simulation and experimental evidence for a conical shaped charge.

The upper bound on the specific internal energy (the value corresponding to the incipient vaporization of the material) in the Tillotson

equation of state for the liner material has been removed in the modified formulation. Now the specific internal energy value used in the pressure calculation is always the value calculated by the algorithm. Since the original formulation used this ad hoc upper bound, the deviation of the pressures, velocities and specific total energies between the two versions is generally small. However, the density values in the modified formulation within the jet are approximately 95% of the initial density, instead of approximately 85% in the original version.

Although a comparison of a conical shaped charge simulation with and without the SPHASE portion of the calculation has not been completed with the modified formulation, the effects of strength should be appreciable since the SPHASE calculation is now included by a significantly larger number of pure cells (mixed cells have no strength). Consequently, simulations performed for detailed jet information should use the strength option.

Besides the obvious effects of an improved internal energy calculation, another effect is the increaseddependence on the material constants used within the code. A case in point is in the shift from the internal energy dependent cut-off value in the SPHASE calculation in the original formulation to a tensile failure criterion in the modified formulation. Thus, the necessity of accurate material constants and models becomes more acute.

As we noted in Sections VI and VII, problems still exist within the HELP code with respect to an accurate internal energy and temperature calculation. The numerical problem related to the computation of negative internal energies along the slipline interface between the copper and explosive as well as in the uncollapsed liner must be corrected. The determination of free surface densities must also be improved. A verified temperature routine incorporated into the modified version of HELP is also needed. Once these are accomplished, the HELP code can be used with confidence to predict not only the jet's shape and jet tip velocity, but also thermodynamic quantities of the jet, such as its density, pressure and temperature.

In the TPHASE section of the original HELP algorithm, the truncation error terms were identified with an explicit artifical viscosity in the internal energy calculation. Consequently, the modified formulation may require implementation of the artificial viscosity option available in HELP in cases where the original formulation did not.

The 1971 version of HELP[8] has a different energy formulation. In SPHASE and HPHASE the specific internal energy was updated directly by a finite difference approximation and the specific total energy was obtained as the sum of the specific internal and kinetic energies. In TPHASE, the specific total energy was updated directly and the specific internal was obtained as the difference of the specific totai and kinetic energies. Although the proposed changes in this report are no longer

directly applicable to such a code, the basic concept developed in this report is: Truncation error terms generated in the calculation of a kinetic energy value from the current values of mass and momentum must be excluded for an acute overall energy calculation.

A noteworth feature of the analysis and modification is that it is directly relevant to codes other than HELP. In fact, any code with a HELP type algorithm can be erroneously affected by the truncation error terms in the kinetic energy calculation. In particular, the same unphysical internal energies in the jet are computed by the HULL code.

A possible alternative solution to the problem discussed in this report is the upgrading of the HELP algorithm to second order accuracy. Such an approach has proven beneficial for the standard particle-in-cell codes.[27] This type of change would require considerable analysis and rewriting of the HELP algorithm. Present problems, which stem primarily from the mixed cell treatment and which may not be solved by a second order algorithm, should be addressed first.

ACKNOWLEDGEMENT

The author wishes to thank Janet M. Lacetera for the many helpful discussions concerning the running of the HELP code.

27. Clark, R., Los Alamos Scientific Laboratory, Private Communication.

REFERENCES

1. Hageman, L. J., et al., "HELP, A Multi-Material Eulerian Program for Compressible Fluid and Elastic-Plastic Flows in Two Space Dimensions and Time," Systems, Science and Software Report No. SSS-R-75-2654, July 1975.

2. Fry, M. A., et al., "The HULL Hydrodynamics Computer Code," Air Force Weapons Laboratory Report No. AFWL-TR-76-193, September 1976.

3. Evans, M. W. and Harlow, F. H., "The Particle-In-Cell Method for Hydrodynamic Calculations," Los Alamos Scientific Laboratory Report No. 2139, November 1957.

4. Harlow, F. H., "The Particle-In-Cell Computing Method for Fluid Dynamics," in Methods in Computational Physics, (B. Alder, S. Fernback and M. Rothenberg, eds.), Academic Press, New York, 1964.

5. Harlow, F. H., "The Particle-In-Cell Method for Numerical Solution of Problems in Fluid Dynamics," in Proceedings of Symposia in Applied Mathematics, Vol. XV, (N. Metropolis, J. Todd, A. Tank, C. Tompkins, eds.) American Mathematical Society, Providence, Rhode Island, 1963.

6. Roache, P. J., Computational Fluid Dynamics, Chapter V, Hermosa, Albuquerque, 1976.

7. Karpp, R. R. and Soldstein, S., "Modifications to the Hydrodynamic Computer Code HELP," Los Alamos Scientific Laboratory Summary Report R199, M-4-1596, December 1977.

8. Hageman, L. J. and Walsh, J. M., "HELP, A Multi-Material Eulerian Program for Compressible Fluid and Elastic-Plastic Flows in Two Space Dimensions and Time, Vol. I, Ballistic Research Laboratory Contract Report No. 39, May 1971. (AD #726459)

9. Control Data Corporation, "UPDATE Reference Manual," Control Data Corporation Manual 60-449900, 1975.

10. Lacetera, J. M., USA Ballistic Research Laboratory, Private Communication, April 1978.

11. Birkhoff, G., et al., "Explosives with Lined Cavities," Journal of Applied Physics 19, 563-582, 1948.

12. Tillotson, J. H., "Metallic Equation of State for Hypervelocity Impact," General Atomic Report No. GA-3216, July 1962.

13. Pugh, E. M., Eichelberger, R. M., and Rostoker, N., "Theory of Jet Formation by Charge with Lined Conical Cavities," Journal of Applied Physics 19, 563-582, 1948.

14. Kiwan, A. R. and Wisniewski, H., "Theory and Computations of Collapse and Jet Velocities of Metallic Shaped Charge Liners," US Army Ballistic Research Laboratory Report No. 1620, 1972. (AD #907161L)

15. Gitting, M. L. "BRLSC: An Advanced Eulerian Code for Predicting Shaped Charges, Volume 1," US Army Ballistic Research Laboratories Contract Report No. 279, December 1975. (AD #A023962)

16. Harrison, J. T., "A Comparison Between the Eulerian Hydrodynamic Computer Code (BRLSC) and Experimental Collapse for a Shaped Charge Liner," US Army Ballistic Research Laboratory Memorandum Report No. ARBAL-MR-02841, June 1978. (AD #A059711)

17. Lee, E., Finger, M. and Collins, W., "JWL Equation of State Coefficients for High Explosives," Lawrence Livermore Laboratory Report No. UCID-16189, January 1973.

18. Lacetera, J., Jr., Lacetera, J. M. and Schmitt, J. A., "The BRL 7600 Version of the HELP Code," USA Ballistic Research Laboratory Report (in preparation).

19. Von Holle, W. G. and Trimble, J. J., "Shaped Charge Temperature Measurements," Proceeding of the Sixth Symposium on Detonation, San Diego, August 1976.

20. Janet, F., "Measure de la densite d'un jet de charge creuse en curvre par radiographic-eclair," Saint-Louis, Rapport-Bericht R 101/76, 9.1.1976.

21. Klem, G. J., US Army Ballistic Research Laboratory, Private Communication, April 1978.

22. Thompson, S. L. and Lauson, H. S., "Improvements in the Chart D Radiation-Hydrodynamic Code III: Revised Analytic Equation of State," Sandia Laboratories Report No. SC-RR-71-0714, March 1972.

23. Edwards, L. L. and Godfrey, C. S., "Computer Code Design of Shaped Charges," Lawrence Livermore Laboratory Report No. UCRL-52598, October, 1978.

24. Wray, W. O. and Cecil, R. A., "Modified Gray: An Improved Three-Phase Equation of State for Metals," US Army Ballistic Research Laboratory Contract Report No. 299, April 1976. (AD #A025260)

25. Von Holle, W. G. and Trimble, J. J., "Temperature Measurement of Copper and Eutectic Metal Shaped Charge Jets," US Army Ballistic Research Laboratory Report No. 2004, 1977. (AD #B021538L)

26. Stull, D. R. and Prophet, H., (project directors), JANAF Thermochemical Tables, 2d ed., June 1971.

27. Clark, R., Los Alamos Scientific Laboratory, Private Communication.

APPENDIX A

LISTING OF MODIFICATIONS TO THE KINETIC ENERGY CALCULATION IN HELP

```
*IDENT KINENGCOR
*I HELPCOM.108
C          ***SDLKFL,SDLKER,SDLKEB,SDLKET ARE KINETIC ENERGIES OF A GIVEN
C             MATERIAL TRANSPORTED ACROSS LEFT,RIGHT,BOTTOM AND TOP
C             BOUNDARIES OFAN INTERFACE CELL
C          ***DLKEL IS KINETIC ENERGY OF MASS TRANSPORTED ACROSS LEFT
C             SIDE OF CELL
*D HELPCOM.112
     4 MFGREZ,REZAMX,REZAIX,REZXMS,REZSIE,REZRHO,SDLKEL,SDLKER,SDLKEB,
     5 S  KET,DLKEL
*D MEMF  ND.45
     3            SFLEFT(4,200),SDLKEL(4,200),SDLKER(4),SDLKEB(4),
     4            SDLKET(4),DLKEL(200)
*I MEMEXPND.59
C          ***TKEG IS SPECIFIC KINETIC ENERGY IN A CELL
C          ***TKEGM IS SPECIFIC KINETIC ENERGY OF MATERIALS IN INTERFACE
C             CELLS
      LEVEL 2,TKEG,TKEGM
      COMMON/KEGCHK/TKEG(12001),TKEGM(4,800)
*D EDIT.17
C          ***USE CORRECT KINETIC ENERGY
      ESUM=ESUM+XMASS(N,M)*(SIE(N,M)+TKEGM(N,M))
*D EDIT.20
C          ***USE CORRECT KINETIC ENERGY
   20 ESUM=ESUM+AMX(K)*(TKEG(K)+AIX(K))
*D EDIT.136
*D EDIT.137
C          ***WRITE CORRECT KINETIC ENERGY
      WRITE(KUNITW) (U(I),V(I),AMX(I),AIX(I),TKEG(I),P(I),MFLAG(I),I=1,
     1 KMAX),(DETIM(I),I=1,KDT)
*D EDIT.146
*D EDIT.147
C          ***WRITE CORRECT KINETIC ENERGY
      WRITE(KUNITW) ((XMASS(M,L),RHO(M,L),SIE(M,L),TKEGM(M,L),US(M,L),
     1 VS(M,L),SAMPY(M,L),SGAMC(M,L),SAMMY(M,L),SAMMP(M,L),M=1,NMAT),
     2 L=1,NMXCLS)
*D EDIT.177
C          ***USE CORRECT KINETIC ENERGY
      WSK=WS*TKEG(K)
*D EDIT.190
C          ***USE CORRECT KINETIC ENERGY
      WSK=WS*TKEGM(M,MC)
*D EQST.124,EQST.130
C          DELETE AD HOC UPPER BOUND ON SPECIFIC INTERNAL ENERGY
C          IN THE PRESSURE CALCULATION FOR THE LINER MATERIAL
*D ENENCHCK.8
C          ***USE CORRECT KINETIC ENERGY
      EKC=AMX(KK2)*TKEG(KK2)
*D ENENCHCK.13
C          ***USE CORRECT KINETIC ENERGY
```

```
      EKM=XMASS(KLM,MBAN)*TKEGM(KLM,MBAN)
*I FILGRD.28
C          ***COMPUTE INITIAL VALUES OF ARRAY TKEGM
      TKEGM(N,M)=0.5*(US(N,M)**2+VS(N,M)**2)
*I FILGRD.32
C          ***USE TKEG AS A STORAGE VARIABLE
      TKEG(K)=TKEG(K)+XMASS(N,M)*TKEGM(N,M)
*I FILGRD.40
C          ***COMPUTE INITIAL VALUES OF ARRAY TKEG FOR MIXED CELL
      TKEG(K)=TKEG(K)/AMX(K)
*I FILGRD.50
C          ***SET MATERIAL KINETIC ENERGY TO CELL KINETIC ENERGY IN
C             NON-SLIP CELLS
      TKEGM(N,M)=TKEG(K)
*I FILGRD.101
C          ***COMPUTE INITIAL VALUES OF ARRAY TKEG FOR PURE CELLS
      TKEG(K)=0.5*(U(K)**2+V(K)**2)
*D FILGRD.123
C          ***USE CORRECT KINETIC ENERGY TO COMPUTE ETH
  162 ETH=ETH+XMASS(N,M)*(SIE(N,M)+TKEGM(N,M))
*D FILGRD.125
C          ***USE CORRECT KINETIC ENERGY TO COMPUTE ETH
  163 ETH=ETH+AMX(K)*(AIX(K)+TKEG(K))
*D FLGSET.51
C          ***USE CORRECT KINETIC ENERGY
      ETH=ETH-XMASS(N,M)*(TKEGM(N,M)+SIE(N,M))
*D FLGSET.55
C          ***USE CORRECT KINETIC ENERGY
      ETH=ETH+XMASS(N,M)*(TKEGM(N,M)+SIE(N,M))
*D HPHASE.168
*D HPHASE.169
C          ***COMPUTE CORRECT CHANGE IN KINETIC ENERGY BY MODELLING THE
C             PARTIAL DIFFERENTIAL EQUATION FOR THE CHANGE OF KINETIC
C             ENERGY IN HPHASE
      DKE=DU*U(K)+DV*V(K)
C          ***COMPUTE CHANGE IN SIE WITH CORRECT DKE
      DIE=DE-DKE
*D HPHASE.181
C          ***DELETE ALTERATIONS TO KINETIC ENERGY AND THUS TO INTERNAL
C             ENERGY DUE TO CHANGES IN THE VELOCITY COMPONENTS IN
C             SUBROUTINE UVCALC
  257 CONTINUE
*D HPHASE.182,HPHASE.184
*D HPHASE.191,HPHASE.196
*I HPHASE.198
C          ***UPDATE THE KINETIC ENERGY OF EACH MATERIAL IN MIXED CELL
      IF (XMASS(N,M).GT.0.) TKEGM(N,M)=TKEGM(N,M)+DKE
*I HPHASE.200
C          ***UPDATE KINETIC ENERGY ARRAY
      TKEG(K)=TKEG(K)+DKE
```

```
*D INPUT.163
*D INPUT.164
C          ***READ THE CORRECT KINETIC ENERGY
      READ (KUNITR) (U(I),V(I),AMX(I),AIX(I),TKEG(I),P(I),MFLAG(I),I=1,
     1 KMAX),(DETIM(I),I=1,KDT)
*D INPUT.173
*D INPUT.174
C          ***READ CORRECT KINETIC ENERGY
      READ (KUNITR) ((XMASS(M,L),RHO(M,L),SIE(M,L),TKEGM(M,L),US(M,L),
     1 VS(M,L),SAMPY(M,L),SGAMC(M,L),SAMMY(M,L),SAMMP(M,L),M=1,NMAT),
     2 L=1,NMXCLS)
*I NEWFLG.16
C          ***SET KINETIC ENERGY OF CELL NOT IN USE TO ZERO
      TKEGM(NN,M)=0.0
*I NEWMIX.14
C          ***DEFINE KINETIC ENERGY FOR NEW MIXED CELL
      TKEGM(MO,M)=TKEG(K)
*D RNDOFF.27
C          ***USE THE CORRECT KINETIC ENERGY
      OUTK=DM*TKEGM(N,M)
*D SETUP.136
*D SETUP.137
C          ***WRITE THE CORRECT KINETIC ENERGY
      WRITE(KUNITW) (U(I),V(I),AMX(I),AIX(I),TKEG(I),P(I),MFLAG(I),I=1,
     1 KMAX),(DETIM(I),I=1,KDT)
*D SETUP.147
*D SETUP.148
C          ***WRITE THE CORRECT KINETIC ENERGY
      WRITE(KUNITW) ((XMASS(M,L),RHO(M,L),SIE(M,L),TKEGM(M,L),US(M,L),
     1 VS(M,L),SAMPY(M,L),SGAMC(M,L),SAMMY(M,L),SAMMP(M,L),M=1,NMAT),
     2 L=1,NMXCLS)
*I SETUPA.112
C          ***INITIALIZE KINETIC ENERGY MATERIAL ARRAY
      TKEGM(N,M)=0.0
*I SETUPA.123
C          ***INITIALIZE KINETIC ENERGY GRID ARRAY
      TKEG(K)=0.0
*D SPHASE.628
C          ***COMPUTE CORRECT CHANGE IN KINETIC ENERGY BY MODELLING THE
C             PARTIAL DIFFERENTIAL EQUATION FOR THE CHANGE OF KINETIC
C             ENERGY IN SPHASE
      DKE=DELU*UKT+DELV*VKT
*D SPHASE.629
C          ***COMPUTE CHANGE IN SIE WITH CORRECT DKE
      DIE=DE-DKE
*I SPHASE.644
C          ***UPDATE THE SPECIFIC KINETIC ENERGY OF EACH MATERIAL IN
C             A MIXED CELL
      TKEGM(MM,MKF)=TKEGM(MM,MKF)+DKE
*I SPHASE.654
```

```
C          ***UPDATE KINETIC ENERGY ARRAY
      TKEG(K)=TKEG(K)+DKE
*D SPHASE.690
*D SPHASE.691
C          ***USE CORRECT KINETIC ENERGY
      E=E+XMASS(NN2,MM2)*(TKEGM(NN2,MM2)+SIE(NN2,MM2))
*D SPHASE.694
C          ***USE CORRECT KINETIC ENERGY
  560 E=E+AMX(KK2)*(TKEG(KK2)+AIX(KK2))
*I TPHASE.23
C          ***SET KINETIC ENERGY FLUX OF EACH MATERIAL AT AXIS TO ZERO
      SDLKEL(N,J)=0.
*I TPHASE.61
C          ***SET KINETIC ENERGY FLUX OF CELL AT AXIS TO ZERO
      DLKEL(J)=0.
*I TPHASE.82
C          ***INITIALIZE KINETIC ENERGY FLUX OF EACH MATERIAL AT BOTTOM
C             TO ZERO
      SDLKEB(N)=0.
*D TPHASE.100
C          ***USE CORRECT KINETIC ENERGY FOR BOTTOM FLUX OF PURE CELL
      DLKEB=TKEG(K)*AMMY
      DELEBK=DLKEB
*I TPHASE.105
C          ***INITIALIZE KINETIC ENERGY FLUX AT BOTTOM
      DLKEB=0.
*I TPHASE.113
C          ***USE CORRECT KINETIC ENERGY FOR BOTTOM FLUX OF EACH MATERIAL
      SDLKEB(N)=TKEGM(N,M)*SAMMY(N,M)
*D TPHASE.114
C          ***USE CORRECT KINETIC ENERGY FLUX OF EACH MATERIAL TO
C             DETERMINE FLUX OF WHOLE CELLFOR KINETIC AND TOTAL
C             ENERGY FLUXES
      DLKEB=DLKEB+SDLKEB(N)
      DELEB=DELEB+SDELEB(N)+SDLKEB(N)
*D TPHASE.116
C          ***USE CORRECT KINETIC ENERGY FOR OUTFLOW OF KINETIC ENERGY
C             AT BOTTOM OF GRID
      OUTKE(N)=OUTKE(N)-SDLKEB(N)
*I TPHASE.149
C          ***SET CORRECT KINETIC ENERGY FLUX AT BOTTOM TO ZERO
      DLKEB=0.
*I TPHASE.158
C          ***INITIALIZE SPECIFIC KINETIC ENERGY FLUXES AT TOP
C             AND RIGHT  TO ZERO
      EKAMPY=0.0
      EKAMMP=0.0
*D TPHASE.218
C          ***USE CORRECT KINETIC ENERGY TO DETERMINE SPECIFIC  KINETIC
C             ENERGY FLUX
```

```
      EKAMPY=TKEGM(MFK,MFL-100)
C          ***USE CORRECT KINETIC ENERGY TO DETERMINE SPECIFIC TOTAL
C             ENERGY FLUX
      EAMPY=SIE(MFK,MFL-100)+EKAMPY
*D TPHASE.227
C          ***USE CORRECT KINETIC ENERGY TO DETERMINE SPECIFIC  KINETIC
C             ENERGY FLUX
  330 EKAMPY=TKEG(M)
C          ***USE CORRECT KINETIC ENERGY TO DETERMINE SPECIFIC TOTAL
C             ENERGY FLUX
      EAMPY=AIX(M)+EKAMPY
*I TPHASE.236
C          ***USE CORRECT KINETIC ENERGY FLUX TO FIND FINAL VALUE AT TOP
      DLKET=AMPY*EKAMPY
*D TPHASE.239
C          ***USE CORRECT KINETIC ENERGY FOR OUTFLOW OF KINETIC ENERGY
C             AT TOP OF GRID
      OUTKE(MFK)=OUTKE(MFK)+AMPY*TKEG(M)
*D TPHASE.293
C          ***USE CORRECT KINETIC ENERGY TO DETERMINE SPECIFIC  KINETIC
C             ENERGY FLUX AT RIGHT FOR MIXED CELL
      EKAMMP=TKEGM(MFK,MFL-100)
C          ***USE CORRECT KINETIC ENERGY TO DETERMINE SPECIFIC TOTAL
C             ENERGY FLUX FOR MIXED CELL
      EAMMP=SIE(MFK,MFL-100)+EKAMMP
*D TPHASE.301
C          ***USE CORRECT KINETIC ENERGY TO DETERMINE SPECIFIC  KINETIC
C             ENERGY FLUX AT RIGHT FOR PURE  CELL
  460 EKAMMP=TKEG(M)
C          ***USE CORRECT KINETIC ENERGY TO DETERMINE SPECIFIC TOTAL
C             ENERGY FLUX FOR PURE CELL
      EAMMP=AIX(M)+EKAMMP
*I TPHASE.311
C          ***USE CORRECT KINETIC ENERGY FLUX TO FIND FINAL VALUE AT RT.
      DLKER=AMMP*EKAMMP
*D TPHASE.314
C          ***USE CORRECT KINETIC ENERGY FOR OUTFLOW OF KINETIC ENERGY AT
C             RIGHT OF GRID
      OUTKE(MFK)=OUTKE(MFK)+AMMP*TKEG(M)
*I TPHASE.319
C          ***INITIALIZE TOP AND RIGHT FLUXES OF KINETIC ENERGY TO ZERO
      DLKET=0.
      DLKER=0.
*I TPHASE.341
C          ***USE CORRECT KINETIC ENERGY FOR KINETIC ENERGY FLUX
      EKAMPY=TKEG(KT)
*I TPHASE.344
C          ***USE CORRECT KINETIC ENERGY FOR KINETIC ENERGY FLUX
      EKAMPY=TKEGM(N,MT)
*I TPHASE.356
```

```
C          ***USE CORRECT KINETIC ENERGY FOR KINETIC ENERGY FLUX
      EKAMMP=TKEG(KR)
*I TPHASE.359
C          ***USE CORRECT KINETIC ENERGY FOR KINETIC ENERGY FLUX
      EKAMMP=TKEGM(N,MR)
*D TPHASE.362
*D TPHASE.363
          ***USE CORRECT SPECIFIC KINETIC ENERGY FLUXES
  560 WSA=EKAMPY
      WSB=EKAMMP
*I TPHASE.365
C          ***INITIALIZE MIXED CELL TRANSPORT VARIABLES
      SDLKET(N)=0.
      SDLKER(N)=0.
*D TPHASE.384
C          ***COMPUTE CORRECT KINETIC ENERGY FLUX FOR EACH MATERIAL
      SDLKET(N)=SAMPY(N,MK)*WSA
C          ***COMPUTE CORRECT TOTAL ENERGY FLUX
      DELET=DELET+SDELET(N)+SDLKET(N)
C          ***COMPUTE CORRECT KINETIC ENERGY FLUX OF CELL
      DLKET=DLKET+SDLKET(N)
*D TPHASE.397
C          ***COMPUTE CORRECT KINETIC ENERGY FLUX FOR EACH MATERIAL
      SDLKER(N)=SAMMP(N,MK)*WSB
C          ***COMPUTE CORRECT TOTAL ENERGY FLUX
      DELER=DELER+SDELER(N)+SDLKER(N)
C          ***COMPUTE CORRECT KINETIC ENERGY FLUX OF CELL
      DLKER=DLKER+SDLKER(N)
*D LCHANGE.16
*D TPHASE.430
C          ***USE CORRECT KINETIC ENERGY FOR OUTFLOW OF KINETIC ENERGY AT
C             TOP OF GRID
  620 OUTKE(N)=OUTKE(N)+SDLKET(N)
*I TPHASE.436
C          ***SET KINETIC ENERGY FLUX TO ZERO
      DLKET=0.0
*D LCHANGE.17
*D TPHASE.457
C          ***USE CORRECT KINETIC ENERGY FOR OUTFLOW OF KINETIC ENERGY AT
C             BOTTOM OF GRID
  660 OUTKE(N)=OUTKE(N)+SDLKEB(N)
*I TPHASE.462
C          ***SET KINETIC ENERGY FLUX TO ZERO
      DLKER=0.0
*D TPHASE.465
C          ***USE CORRECT KINETIC ENERGY
      WSA=TKEG(K)
*I TPHASE.467
C          ***COMPUTE TOTAL CHANGE IN KINETIC ENERGY FOR PURE CELL
      SIGKE=-DLKET-DLKER+DLKEB+DLKEL(J)
```

```
*I TPHASE.470
C          ***INITIALIZE VALUE OF EKNEW TO ZERO
      EKNEW=0.
*I TPHASE.473
C          ***COMPUTE NEW VALUE OF KINETIC ENERGY FOR PURE CELL
      EKNEW=(SIGKE+AMX(K)*TKEG(K))/WS
*I TPHASE.486
C          ***COMPUTE NEW VALUE OF KINETIC ENERGY FOR MIXED CELL
      SSIGKE=-SDIKET(N)-SDLKER(N)+SDLKEL(N,J)+SDLKEB(N)
*I TPHASE.492
C          ***SET KINETIC ENERGY OF CELL TO ZERO
      TKEGM(N,MK)=0.
*I TPHASE.500
C          ***TRANSFER CORRECT KINETIC ENERGY VALUE
      EKNW=EKNEW
*I TPHASE.503
C          ***COMPUTE TOTAL CHANGE IN KINETIC ENERGY FOR MIXED CELL
      EKNW=(SSIGKE+XMASS(N,MK)*TKEGM(N,MK))/SWS
*D TPHASE.504,TPHASE.516
C          ***LINES 504-516 WERE DELETED SINCE KINETIC ENERGY EQUATION
C             IS BEING MODELLED AND THERMALIZED ENERGY IS A PROPERTY OF
C             ORIGINAL SCHEME
  720 SWSA=(SIE(N,MK)*XMASS(N,MK)+SWSB)/SWS
*I TPHASE.525
C          ***SET COMPUTED KINETIC ENERGY TO ARRAY VALUE FOR A MIXED CELL
      TKEGM(N,MK)=EKNW
*D TPHASE.538
C          ***COMPUTE NEW VALUE OF INTERNAL ENERGY BASED ON CORRECT K.E.
      SIENEW=(AIX(K)*AMX(K)+WSB-SIGKE)/WS
*I TPHASE.547
C          ***SET COMPUTED KINETIC ENERGY TO ARRAY VALUE FOR A PURE CELL
      TKEG(K)=EKNEW
*D TPHASE.569
C          ***COMPUTE TOTAL ENERGY IN GRID WITH CORRECT KINETIC ENERGY
      ENEPGY=ENERGY+AMX(LJD)*(AIX(LJD)+TKEG(LJD))
*D TPHASE.564
*D TPHASE.565
C          ***COMPUTE TOTAL  ENERGY IN GRID WITH CORRECT KINETIC ENERGY
      ENERGY=ENERGY+XMASS(NJ,MJ)*(SIE(NJ,MJ)+TKEGM(NJ,MJ))
*I TPHASE.573
C          ***WRITE KINETIC ENERGY FLUXES FOR CELL CENTERED QUANTITIES
      WRITE (6,1330) DLKET,DLKER,DLKEB,DLKEL(J)
*I TPHASE.582
C          ***WRITE KINETIC ENERGY FLUXES FOR EACH MATERIAL IN MIXED CELL
      WRITE (6,1340) (N,SDLKET(N),SDLKER(N),SDLKEB(N),SDLKEL(N,J),N=1,NM
     1AT)
*I TPHASE.588
C          ***SET KINETIC ENERGY FLUXES TO ZERO FOR EACH MATERIAL
      SDLKEB(N)=0.
      SDLKEL(N,J)=0.
```

```
*I TPHASE.608
C          ***STORE FLUXES TO BE USED IN TRANSPORT OF KINETIC ENERGY
      SDLKEB(N)=SDLKET(N)
      SDLKEL(N,J)=SDLKER(N)
*I TPHASE.626
C          ***STORE FLUXES FOR KINETIC AND INTERNAL ENERGIES WHICH USE
C             CORRECT KINETIC ENERGY
      SDLKEB(MFK)=EKAMPY*AMPY
      SDELEB(MFK)=DELET-SDLKEB(MFK)
*I TPHASE.633
C          ***STORE FLUXES FOR KINETIC AND INTERNAL ENERGIES WHICH USE
C             CORRECT KINETIC ENERGY
      SDLKEL(MFK,J)=EKAMMP*AMMP
      SSIGC(MFK,J)=DELER-SDLKEL(MFK,J)
*I TPHASE.643
C          ***STORE KINETIC ENERGY FLUX
      DLKEL(J)=DLKER
*I TPHASE.647
C          ***STORE KINETIC ENERGY FLUX
      DLKEB=DLKET
*D TPHASE.698
C          ***USE CORRECT KINETIC ENERGY
      WS=TKEG(K)
*I TPHASE.715
C          ***INITIALIZE KINETIC ENERGY SUM TO ZERO
      EKSUM=0.
*D TPHASE.728
C          ***USE CORRECT KINETIC ENERGY
      WS=TKEGM(N,M)
*I TPHASE.740
C          ***SET KINETIC ENERGY OF MIXED CELL TO ZERO
      TKEGM(N,M)=0.
*I TPHASE.744
C          ***SUM KINETIC ENERGIES
      EKSUM=EKSUM+TKEGM(N,M)*XMASS(N,M)
*I TPHASE.753
C          ***DEFINE KINETIC ENERGY OF CELL
      TKEG(K)=EKSUM/XMSUM
*I TPHASE.758
C          ***SET KINETIC ENERGY OF CELL TO ZERO
      TKEG(K)=0.
*I TPHASE.771
C          ***SET KINETIC ENERGY OF MIXED CELL TO ZERO
      TKEGM(N,MK)=0.
*I TPHASE.781
C          ***SET KINETIC ENERGY OF CELL TO ZERO
      TKEG(K)=0.
*I TPHASE.857
 1330 FORMAT (7H DLKET=1PE15.8,6X,6HDLKER=1PE15.8,6X,6HDLKEB=1PE15.8,10H
     1 DLKEL(J)=1PE15.8)
```

```
 1340 FORMAT (I3,8H SDLKET=1PE15.8,6X,7HSDLKER=1PE15.8,6X,7HSDLKEB=1PE15
     1.8,6X,7HSDLKEL=1PE15.8)
*D UVMOD.69
C          ***DELETE ALTERATIONS TO KINETIC ENERGY AND THUS TO INTERNAL
C             ENERGY DUE TO CHANGES IN THE VELOCITY COMPONENTS IN
C             SUBROUTINE UVMOD
C          ***LINES 69,70,82,83,85,87-91 OF UVMOD WERE DELETED
*D UVMOD.70
*D UVMOD.82
*D UVMOD.83
*D UVMOD.85
   40 CONTINUE
*D UVMOD.87,UVMOD.91



*ID CORMAP
*D MAP.13
      DATA XUM /2H .,2H—,2H-A,2H-B,2H-C,2H-D,2H-E,2H-F,2H-G,2H-H,2H-I,2
```

APPENDIX B

LISTING OF REZONING ROUTINE AND MODIFICATIONS

```
*ID REZJAS
*D MAIN.23
C     REZONE AT CYCLE REYC9
C      USER MUST SUPPLY REYC9 IN NEXT STATEMENT
       IF(NC .NE.  REYC9) GO TO 30
*IDENT CHREZ
*D REZONE.159,REZONE.160
C     SET NJMAX=JEXTY WHERE JEXTY = THE NUMBER OF ROWS TO BE REZONED
       NJMAX=JEXTY
       IF (MOD(JEXTY,2) .EQ. 0) GO TO 210
*D REZONE.172
  210 NJMAX1=NJMAX/2
       NJMAX3=NJMAX+1
*D REZONE.182
       IF (I.GE. NJMAX) GO TO 225
       IF (I .LT. NJMAX .AND. IVARDY .EQ. 1) GO TO 220
*I REZONE.188
       GO TO 230
  225 TY(N,M)=TY(N,M)-NJMAX1
*D REZONE.196
       IF(I .GE. NJMAX) GO TO 255
       IF(I.LT. NJMAX .AND. IVARDY.EQ. 1) GO TO 250
*I REZONE.202
  255 YP(M)=YP(M)-NJMAX1
*D REZONE.238
       DO 320 J=1,NJMAX1
*I REZONE.244
       NJMAX2=NJMAX1+1
       DO 324 J=NJMAX3,JMAX
       DO 325 I=1,IMAX
       K=(NJMAX2-1)*IMAX+I+1
       M=(J-1)*IMAX+I+1
       MFLAG(K)=MFLAG(M)
       AIX(K)=AIX(M)
       U(K)=U(M)
       V(K)=V(M)
       TKEG(K)=TKEG(M)
        AMX(K)=AMX(M)
       IF(CYCPH3 .LT. 0) GO TO 326
       STRSRR(K)=STRSRR(M)
       STRSRZ(K)=STRSRZ(M)
       STRSZZ(K)=STRSZZ(M)
  326 IF(IDRT .LE. 0) GO TO 327
       DETIM(K)=DETIM(M)
C      **    ZERO OUT ORGINAL CELL  ***
  327 AIX(M)=0.0
       AMX(M)=0.0
       U(M)=0.0
       V(M)=0.0
       TKEG(M)=0.0
```

```
      IF(IDRT .LE. 0) GO TO 328
       DETIM(M)=0.0
  328 IF (CYCPH3 .LT. 0) GO TO 329
      STRSRR(M)=0.0
      STRSRZ(M)=0.0
      STRSZZ(M)=0.0
  329 CONTINUE
  325 CONTINUE
      NJMAX2=NJMAX2+1
  324 CONTINUE
*D REZONE.248
      DO 330 J=1,NJMAX1
*D REZONE.250,REZONE.251
      NJMAX2=NJMAX1+1
      NJMAXS=NJMAX
      NJMAX4=JMAX-NJMAX1
      DO 340 J=NJMAX2,NJMAX4
      Y(J)=Y(NJMAXS+1)
  340 NJMAXS=NJMAXS+1
      NJMAX5=NJMAX4+1
      YDELT=Y(NJMAX4)-Y(NJMAX4-1)
      DO 345 J=NJMAX5,JMAX
  345 Y(J)=Y(J-1)+YDELT
*I REZONE.257
      DO 370 J=NJMAX5,JMAX
*D REZONE.259
*D REZONE.282
      DO 380 J=NJMAX5,JMAX
*D REZONE.285,REZONE.287
      I2=NJMAX5+2
      IF (JDBT .GT. 0) JDBT=NJMAX5+1
      IF (JTYP .GT. 0) JDTP=NJMAX5+1
*D REZONE.303
     1TY=,I5,/)
```

```
*IDENT CORREZ
*D MEMEXPND.58
     3               REZRHO(4,200),TTKM(2,4)
*I REZONE.133
      TKEG(K)=0.0
*I REZONE.141
      TKEGM(N,MFK)=0.0
*I REZONE.265
      TKEG(K)=0.0
*I REZONE.274
      TKEGM(N,MFK)=0.0
```

```
*D COMPRS.26,COMPRS.30
*B COMPRS.31
      AIX(K)=(AIX(L)*AMX(L)+AIX(M)*AMX(M))/WSA
      TKEG(K)=(TKEG(L)*AMX(L)+TKEG(M)*AMX(M))/WSA
*I COMPRS.48
      TKEG(M)=0.0
*I COMPRS.59
      TKEG(L)=0.0
*I COMPRS.80
      TTKM(II,JJ)=0.0
*I COMPRS.103
      TTKM(JJ,II)=TKEGM(II,N)
*I COMPRS.109
      TKEGM(II,N)=0.0
*I COMPRS.126
      TTKM(1,MFM)=TKEG(M)
*I COMPRS.138
      TTKM(2,MFL)=TKEG(L)
*I COMPRS.152
      TKEG(K)=0.0
*D COMPRS.165,COMPRS.170
*B COMPRS.171
      SIE(II,N)=(SSIE(1,II)*XMAS(1,II)+SSIE(2,II)*XMAS(2,II))/WSB
      TKEGM(II,N)=(TTKM(1,II)*XMAS(1,II)+TTKM(2,II)*XMAS(2,II))/WSB
*I COMPRS.173
      TKEG(K)=TKEG(K)+TKEGM(II,N)*XMASS(II,N)
*I COMPRS.177
      TKEG(K)=TKEG(K)/WSA
*D COMPRS.184
*D COMPRS.185
*I COMPRS.181
      TKE=0.0
*I COMPRS.186
      TKE=TKE+TKEGM(II,N)*XMASS(II,N)
*I COMPRS.191
      TKEG(K)=TKE/WSA
```

APPENDIX C

LISTING OF TEMPERATURE AND SPECIAL PRINTING ROUTINE

The HULL temperature routine uses the absolute specific internal energy value and not the specific internal energy value above the initial value. Consequently, this routine augments the specific internal energy value from the HELP code by 0.113335748 MJ/kg which corresponds to a temperature of 287.87K at ambient pressure of 0.101325 MPa and ambient density of 8.9×10^3 kg/m^3. The routine has two purposes: to calculate a temperature value for the copper material according to the HULL temperature routine and to list the cell values of certain quantities associated with the copper material. It was appended to the MAIN subroutine by an UPDATE directive INSERT.

```
*ID HULLTEMP
*I MAIN.16
      WRITE(6,1025)
 1025 FORMAT(1H1,5X,1HI,3X,1HJ,6X,4HMASS,9X,5HU-VEL,8X,5HV-VEL,9X,3HSIE,
     *10X,3HSKE,8X,7HU2+V2/2,6X,7HDENSITY,7X,4HTEMP,10X,3HSTE)
      REFRHO=8.9
      F1=-1285.
      F2=-10000.
      F3=2.54E-07
      F4=1.63E-07
      EMP=1.41E10
      ES=5.31E10
      DO 1021 I=1,IMAX
      DO 1021 J=1,JMAX
      K=(J-1)*IMAX+I+1
      IF (MFLAG(K) .GT. 100) GO TO 1023
      IF (MFLAG(K) .NE.1) GO TO 1021
C  PURE CELL
      SKE=0.5*(U(K)**2+V(K)**2)
      E=AIX(K)
      DENSITY=AMX(K)/(TAU(I)*DY(J))
      KEY=1
      GO TO 1031
 1032 CONTINUE
      TENG=AIX(K)+TKEG(K)
      WRITE(6,1022)I,J,          AMX(K),U(K),V(K),AIX(K),TKEC(K),SKE,
     * DENSITY,TEMP,TENG
 1022 FORMAT(1H ,1HP,       2(1X,I4),9(1X,1PE12.4))
      GO TO 1021
C  MIXED CELL
 1023 M=MFLAG(K)-100
      IF(SIE(1,M) .EQ. 0.0) GO TO 1021
      N=1
      SKE=0.5*(US(N,M)**2+VS(N,M)**2)
      DENSITY=RHO(1,M)
```

```
      E=SIE(1,M)
      KEY=2
      GO TO 1031
 1033 CONTINUE
 1027 TENG=SIE(N,M)+TKEGM(N,M)
      WRITE (6,1024) I,J,  XMASS(N,M),US(N,M),VS(N,M),SIE(N,M),TKEGM(N,M
     * ),SKE, DENSITY,TEMP,TENG
 1024 FORMAT (1H ,1HM,     2(1X,I4),9(1X,1PE12.4) )
      GO TO 1021
 1031 CONTINUE
C  HULL TEMPERATURE ROUTINE
      E=E+1.13335748E9
      RMU=DENSITY/REFRHO-1
      RMU=AMAX1(RMU,-1.0)
      RMU=AMIN1(RMU,0.679)
      S=AMAX1((E-EMP)*1.E-03,0.0)
      EE=AMIN1(E,EMP+AMAX1(E-EMP-ES,S))
      IF(RMU.LT.0.0) GOTO 100
      CON1=(F2*RMU+F1)*RMU
      CON2=F3
      GOTO 200
  100 CON1=0.0
      CON2=F3+F4*RMU
  200 TEMP=CON1+CON2*EE
      DTDE=CON2
      IF(E.GT.EMP.AND.E.LT.(EMP+ES))DTDE=DTDE*1.0E-03
      IF(TEMP .GE.10.0) GO TO 11
      IF(CON1.EQ.0.0) GOTO 11
      CON2=10.0*CON2/(10.0-CON1)
      TEMP=CON2*E
      DTDE=CON2
   11 CONTINUE
      IF ( KEY .EQ. 1) GOTO 1032
      GO TO 1033
 1021 CONTINUE
```

LIST OF SYMBOLS

e - specific kinetic energy (J/kg)

m - mass per unit length (kg/m)

t - time (s)

u - x-component of velocity (m/s)

v - y-component of velocity (m/s)

x - Cartesian spatial coordinate (m)

y - Cartesian spatial coordinate (m)

A - cross sectional area of computational cell (m^2)

B - boundary of computational cell traversed in a positive sense (m)

E - specific total energy (J/kg)

I - specific internal energy (J/kg)

L - length of cell boundary (m)

O - order symbol

P - pressure (Pa)

S - stress deviator tensor (Pa)

δm - transported mass per unit length (kg/m)

λ - $0.5\rho u\Delta x$

λ' - $0.5\rho u^2\Delta t$

ρ - density (kg/m^3)

Δt - time increment (s)

Δx - grid increment in the x-direction (m)

Δy - grid increment in the y-direction (m)

SUBSCRIPTS

i - denotes the number of the cell in the x-direction

j - denotes the number of the cell in the y-direction

n - denotes the number of time increments

SUPERSCRIPTS

a - denotes the computational cell boundary above its center

b - denotes the computational cell boundary below its center

d - denotes generic computational cell boundary

ℓ - denotes the computational cell boundary to the left of its center

r - denotes the computational cell boundary to the right of its center

~ - denotes value of a variable at the completion of SPHASE

— - denotes value of a variable at the completion of HPHASE

DISTRIBUTION LIST

No. of Copies	Organization
12	Commander Defense Documentation Center ATTN: DDC-DDA Cameron Station Alexandria, VA 22314
1	Director Defense Research and Engineering ATTN: Tech Lib, Rm 3D-1039 Washington, DC 20301
1	Director Defense Advanced Research Projects Agency ATTN: Dr. Ernest F. Blase 1400 Wilson Boulevard Arlington, VA 22209
1	Commander US Army Materiel Development and Readiness Command ATTN: DRCDMD-ST 5001 Eisenhower Avenue Alexandria, VA 22333
1	Commander US Army Aviation Research and Development Command ATTN: DRSAV-E P. O. Box 209 St. Louis, MO 63166
1	Director US Army Mobility Research and Development Laboratory Ames Research Center Moffett Field, CA 94035
1	Commander US Army Electronics Research and Development Command Technical Support Activity ATTN: DELSD-L Fort Monmouth, NJ 07703
1	Commander US Army Communications Rsch and Development Command ATTN: DRDCO-PPA-SA Fort Monmouth, NJ 07703
2	Commander US Army Missile Research and Development Command ATTN: DRDMI-R DRDMI-YDL Redstone Arsenal, AL 35809
1	Commander US Army Tank Automotive Research & Development Cmd ATTN: DRDTA-UL Warren, MI 48090
7	Commander US Army Armament Research and Development Command ATTN: Dr. N. Clark Mr. G. Randers-Pehrson Mr. J. Pearson Mr. J. Hershkowitz Mr. A. Anzalone DRDAR-TSS (2 cys) Dover, NJ 07801
8	Commander US Army Armament Research and Development Command ATTN: DRDAR-SC/Mr. Hirshman Mr. F. Puzycki DRDAR-SCN/Mr. Kahn DRDAR-SCW/Mr. Townsend DRDAR-LC-F/Mr. Loeb Mr. E. Friedman DRDAR-LCV/Mr. Barrieres Mr. Reisman Dover, NJ 07801

DISTRIBUTION LIST

No. of Copies	Organization
1	Commander US Army Armament Materiel Readiness Command ATTN: DRSAR-LEP-L, Tech Lib Rock Island, IL 61299
1	Commander Benet Weapons Laboratory US Army Armament Research and Development Command ATTN: DRDAR-LCB-TL SARWV-PDR-S/S.Sautter SARWV-PDR-AMM/Dr. Zweig SARWV-RDD-SE/P.A.Alto Watervliet, NY 12189
1	Commander US Army Jefferson Proving Ground ATTN: STEJP-TD-D Madison, IN 47250
3	Commander US Army Materials and Mechanics Research Center ATTN: DRXMR-ARL/W. Woods DRXMR-T/J. Mescall Tech Lib Watertown, MA 02172
1	Commander US Army Natick Research and Development Command ATTN: DRXRE/Dr. Sieling Natick, MA 01762
1	Director US Army TRADOC Systems Analysis Activity ATTN: ATAA-SL, Tech Lib White Sands Missile Range NM 88002

No. of Copies	Organization
1	Assistant Secretary of the Army (R&D) ATTN: Asst for Research Washington, DC 20310
2	HQDA (DAMA-ZA; DAMA-AR) Washington, DC 20310
1	Commander US Army Research Office P. O. Box 12211 Research Triangle Park NC 27709
1	Commander US Army Ballistic Missile Defense Systems Command Huntsville, AL 35804
1	Director US Army BMD Advanced Technology Center P. O. Box 1500, West Station Huntsville, AL 35807
2	Chief of Naval Research ATTN: Code 427 Code 470 Department of the Navy Washington, DC 20325
2	Commander Naval Air Systems Command ATTN: Code AIR-310 Code AIR-350 Washington, DC 20360
1	Commander Naval Ordnance Systems Command ATTN: Code ORD-0332 Washington, DC 20360

DISTRIBUTION LIST

No. of Copies	Organization
2	Commander and Director David W. Taylor Naval Ship Research & Development Center ATTN: Tech Library Aerodynamic Lab Bethesda, MD 20084
4	Commander Naval Surface Weapons Center ATTN: Dr. H. Sternberg Mr. W. Walker Dr. J. Coughlin Code 730, Lib Silver Spring, MD 20910
2	Commander Naval Surface Weapons Center ATTN: DG-50/K. Bannister DX-21, Lib Br. Dahlgren, VA 22448
1	Commander Naval Weapons Center ATTN: Code 45, Tech Lib China Lake, CA 93555
1	Commander Naval Research Laboratory Washington, DC 20375
1	Commander Naval Ordnance Station ATTN: Code FS13A/P. Sewell Indian Head, MD 20640
1	USAF/AFRDDA Washington, DC 20330
1	AFSC/SDW Andrews AFB Washington, DC 20331
1	US Air Force Academy ATTN: Code FJS-RL(NC) Tech Lib Colorado Springs, CO 80840
1	AFRPL/LKCB (Dr. Horning) Edwards AFB, CA 93523
1	ADTC (ADBPS-12) Eglin AFB, FL 32542
1	AFATL (Tech Lib) Eglin AFB, FL 32542
1	AFATL/DLJW (CPT R. Bell) Eglin AFB, FL 32542
1	AFATL/DLJW (Mr. Beech) Eglin AFB, FL 32542
1	AFWL (SUL, LT Tennant) Kirtland AFB, NM 87116
1	AFAL/AVW Wright-Patterson AFB, OH 45433
1	AFLC/MMWMC Wright-Patterson AFB, OH 45433
1	ASD/XRA (Stinfo) Wright-Patterson AFB, OH 45433
1	Director US Bureau of Mines ATTN: Mr. R. Watson 4800 Forbes Street Pittsburgh, PA 15213
4	Director Lawrence Livermore Laboratory ATTN: Dr. M. Wilkins Dr. J. Kury Dr. E. Lee Dr. H. Horning P. O. Box 808 Livermore, CA 94550

DISTRIBUTION LIST

No. of Copies	Organization
3	Director Lawrence Livermore Laboratory ATTN: E. D. Giroux G. L. Goudreau Tech Lib P. O. Box 808 Livermore, CA 94550
1	Director NASA Scientific and Technical Information Facility ATTN: SAK/DL P. O. Box 8757 Baltimore/Washington International Airport, MD 21240
1	Director Jet Propulsion Laboratory ATTN: Tech Lib 2800 Oak Grove Drive Pasadena, CA 91103
1	Director National Aeronautics and Space Administration Langley Research Center ATTN: MS 185/Tech Lib Hampton, VA 23365
1	Director National Aeronautics and Space Administration Lewis Research Center 21000 Brookpark Road Cleveland, OH 44135
1	Director National Aeronautics and Space Administration George C. Marshall Space Flight Center ATTN: MS-I/Lib R-AERO-AE/A. Felix Huntsville, AL 35812
1	AAI Corporation ATTN: Dr. T. Stastny Cockeysville, MD 21030
1	Advanced Technology Labs ATTN: Dr. J. Erdos Merrick & Stewart Avenues Westbury, NY 11590
1	Aerospace Corporation ATTN: Dr. T. Taylor P. O. Box 92957 Los Angeles, CA 90009
2	ARO, Inc. ATTN: Tech Lib Dr. J. Adams Arnold AFS, TN 37389
1	ARTEC Associates, Inc. ATTN: Dr. S. Gill 26046 Eden Landing Road Hayward, CA 94545
1	AVCO Systems Division ATTN: Dr. W. Reinecke 201 Lowell Street Wilmington, MA 01887
1	Battelle Columbus Laboratories 505 King Avenue Columbus, OH 43201
1	Calspan Corporation P. O. Box 235 Buffalo, NY 14221
1	General Electric Corporation Armaments Division ATTN: Mr. R. Whyte Lakeside Avenue Burlington, VT 05401

DISTRIBUTION LIST

No. of Copies	Organization
1	Lockheed Missiles and Space Company ATTN: Mr. J. E. May 55-80 Bldg 57 P. O. Box 504 Sunnyvale, CA 94088
1	Martin Marietta Aerospace ATTN: Mr. A. J. Culotta P. O. Box 5378 Orlando, FL 32805
1	Orlando Technology Inc. ATTN: Mr. D. Matuska P. O. Box 855 Shalimar, FL 32579
1	Physics International Corpo ATTN: Mr. L. Behrmann 2700 Merced Street San Leandro, CA 94577
1	Rockwell International Science Center ATTN: Dr. Norman Malmuth P. O. Box 1085 1000 Oaks, CA 91360
1	S&D Dynamics, Inc. ATTN: Dr. M. Soifer 755 New York Avenue Huntington, NY 11743
2	Sandia Laboratories ATTN: Dr. W. Herrmann Dr. L. Bertholf Albuquerque, NM 87115
1	Shock Hydrodynamics ATTN: Dr. L. Zernow 4710-4716 Vineland Avenue N. Hollywood, CA 91602
1	Systems, Science & Software ATTN: Dr. R. Sedgwick P. O. Box 1620 La Jolla, CA 92037
1	California Institute of Tech Guggenheim Aeronautical Lab ATTN: Tech Lib Pasadena, CA 91104
2	Drexel Institute of Tech Wave Propagation Research Ctr ATTN: Prof. P. Chou Dr. J. Carleone 32d & Chestnut Streets Philadelphia, PA 19104
1	Franklin Institute ATTN: Dr. Carfagno Dr. Wachtell Race & 20th Streets Philadelphia, PA 19103
1	Director Applied Physics Laboratory The Johns Hopkins University Johns Hopkins Road Laurel, MD 20810
1	Oregon State College Department of Mathematics ATTN: Prof. D. Jesperson Corvallis, OR 97331
1	Polytechnic Institute of Brooklyn Graduate Center ATTN: Tech Lib Farmingdale, NY 11735
1	Forrestal Campus Library Princeton University P. O. Box 710 Princeton, NJ 08540

DISTRIBUTION LIST

No. of Copies	Organization
1	Southwest Research Institute ATTN: Mr. Peter S. Westine P. O. Drawer 28510 8500 Culebra Road San Antonio, TX 78228
1	SRI International ATTN: Dr. A. Florence Poulter Laboratories Menlo Park, CA 94025
4	University of California Los Alamos Scientific Lab ATTN: Dr. J. Walsh Dr. R. Karpp Dr. R. Clark Tech Lib P. O. Box 1663 Los Alamos, NM 87545
1	Mathematics Research Center University of Wisconsin-Madison 610 Walnut Street Madison, WI 53706
1	Washington State University Department of Physics ATTN: Prof. G. Duvall Pullman, WA 99163

Aberdeen Proving Ground

Dir, USAMSAA
ATTN: Dr. J. Sperrazza
DRXSY-MP, H. Cohen
Cdr, USATECOM
ATTN: DRSTE-TO-F
Dir, Wpns Sys Concepts Team
Bldg. E3516, EA
ATTN: DRDAR-ACW